ELSEVIER

Chemical Engineering Journal 137 (2008) 102–121

Chemical Engineering Journal

www.elsevier.com/locate/cej

In vivo and *in vitro* applications of collagen-GAG scaffolds

Brendan A.C. Harley [a], Lorna J. Gibson [b,*]

[a] *Joint Program in Transfusion Medicine, Children's Hospital, Boston, MA 02115, United States*
[b] *Department of Materials Science and Engineering, Massachusetts Institute of Technology, 77 Massachusetts Avenue, Room No. 3-240, Cambridge, MA 02139, United States*

Received 4 June 2007; received in revised form 17 August 2007; accepted 3 September 2007

Abstract

Tissue engineering scaffolds are used extensively as three-dimensional analogs of the extracellular matrix (ECM). Collagen-glycosaminoglycan (CG) scaffolds have long been utilized as ECM analogs for the regeneration of skin and are currently being considered for the regeneration of nerve, conjunctiva, and a host or orthopedic tissues. Recently a series of CG scaffolds with a uniform pore microstructure has been developed with a range of sizes of equiaxed pores. Experimental characterization and theoretical modeling techniques have been used to describe the pore microstructure, specific surface area, tensile and compressive mechanical properties, cell attachment, and permeability of these variants. Here we describe the fabrication, and characterization, and modeling of a series of CG and mineralized CG scaffolds. We then discuss their use *in vivo* to induce tissue regeneration following injury and *in vitro* as standardized 3D materials to study the influence of microstructural and mechanical features on cell behaviors such as motility and contraction.

Keywords: Scaffolds; Tissue engineering; Collagen; Cellular solids

1. Introduction

The extracellular matrix (ECM) is a complex organization of structural proteins such as collagens and a wide variety of proteoglycans that is found within tissues and organs. The ECM forms a fibrillar network that acts as an insoluble regulator of cell behavior; among other things, the ECM plays a significant role in defining the overall mechanics of a tissue, is responsible for conducting mechanical stimuli from the organ-scale to individual cells, can influence cell behavior through integrin-ligand complexes, and can influence delivery of soluble regulators (*i.e.*, cytokines, growth factors, hormones, other paracrine and endocrine signals) through its fibrillar network to target cells. With the understanding that *in situ* cells exist within a complex, three-dimensional structure a wide variety of tissue engineering scaffolds have been created for a multitude of applications. As an analog of the native ECM, the scaffold acts as a physical support structure and insoluble regulator of cell activity. Scaffold microstructure (porosity, mean pore size, pore shape, interconnectivity, specific surface area) [1–6] and mechanical properties (Young's modulus) [7–16] have been shown to significantly influence cell behaviors such as adhesion, growth, and differentiation. Scaffold microstructure and stiffness have also been shown to affect the bioactivity of scaffolds used for *in vivo* tissue regeneration applications [1].

The primary application of porous biomaterials has been *in vivo* as a regeneration template to induce a modification in the characteristic healing process following injury. Increasing, scaffolds have also been used *in vitro* as a controlled three-dimensional environment to probe cell-scaffold interactions and the ways in which cell behavior may be governed by its local environment. There are three major classifications of chemical compositions (and composites thereof) that have been utilized to produce scaffolds for tissue engineering applications: synthetic polymers, inorganic materials, and organic polymers. Inorganic–organic composites and naturally derived ECMs will also be briefly described here. We will first describe these general material classifications and then will focus on the *in vivo* and *in vitro* applications of collagen-glycosaminoglycan scaffolds.

* Corresponding author. Tel.: +1 617 253 2503; fax: +1 617 253 8388.
E-mail address: ljgibson@mit.edu (L.J. Gibson).

1385-8947/$ – see front matter © 2007 Elsevier B.V. All rights reserved.
doi:10.1016/j.cej.2007.09.009

1.1. Synthetic polymers

A wide range of synthetic polymers has been used to fabricate porous scaffolds. These polymers include polylactic acid (PLA, polylactide), its chiral derivative poly-L-lactide (PLLA), polyglycolic acid (PGA, polyglycolide), its copolymer with PLA poly(lactic-co-glycolic acid) (PLGA), ε-caprolactone (ε-CPL) and polycaprolactone, polyethylene (PE), poly(ethylene glycol) (PEG), and copolymers thereof [17–21]. A significant benefit to using synthetic polymers is that a host of processing techniques including those that utilize high temperatures and pressures can be applied to produce porous biomaterials with complex microstructures. These techniques include solid free-form fabrication, electrospinning and other fibrillar molding techniques, as well as a variety of liquid state molding techniques [22]. However, synthetic polymers do not express surface ligands appropriate for cell attachment and therefore require biologically relevant surface coatings. Another area of concern is scaffold degradation; some synthetic polymers are non-degradable while others have cytotoxic degradation byproducts, making their use *in vivo* limited. Finally, like many organic polymers (discussed below), porous biomaterials fabricated from synthetic polymers are often too weak for high load *in vivo* applications. Mechanical considerations can limit their application to soft tissues and those not undergoing large-scale deformation.

1.2. Inorganic materials

Calcium phosphates (CaP) are the primary inorganic materials that have been used to craft porous biomaterials for tissue engineering applications. Calcium phosphates, specifically a biological form of hydroxyapatite, are the major constituent of bone, constituting approximately 75% of its dry mass [23] and are responsible for providing much of its mechanical stiffness and strength. CaP, their derivatives, and composites thereof are often the main component of bone tissue engineering constructs [24–26]. CaP were originally used to improve the chemical interactions between a fixed implant and bone, and their extensive use as bone substitutes has yielded a lucrative commercial market, with products ranging from coatings [27,28] to porous implants [29] to bioactive composites [30,31]. The past 15 years have witnessed the emergence of a vast number of other CaP-based products – including dense bone fillers [32–34], porous implants [29,35], and advanced CaP-based composites [30,31]. When combined with polymeric materials, CaP composites impart high stiffness and compressive strength. As bone substitute materials, they are biocompatible and have the unique capacity to bond directly to bone.

Bioactive glasses are a second type of inorganic materials commonly used to produce porous biomaterials. Bioactive glasses are a group of surface reactive glass-ceramics and include the original bioactive glass, 45S5 Bioglass, that is fabricated from silicone oxide (SiO_2) compounds [36,37]. These materials are formed as a glass and then are partially crystallized via heat treatment to increase their strength. The biocompatibility of these glasses has led them to be investigated extensively for use as implant materials to repair and replace diseased or damaged bone. Porous glass-ceramic scaffolds are typically made as composites with other synthetic materials and are then formed via high pressure and sintering; more recently electrospinning approaches have been utilized to produce fibrillar bioactive glasses that can be formed into a porous composite material [38–40]. However, like CaP-based biomaterials, these bioactive materials are relatively stiff, brittle and difficult to form into complex shapes, particularly as porous scaffolds, making their applications limited *in vivo* [36,41–43].

1.3. Organic polymers

Organic polymers are perhaps the most intriguing materials used to create scaffolds for tissue engineering applications. Like synthetic polymers, scaffolds made from organic polymers typically do not exhibit the requisite mechanical properties for high-strength applications. However, as materials isolated directly from the natural ECM, organic polymers contain a host of surface ligands (*i.e.*, fibronectin, laminin, and vitronectin) and peptides (*i.e.*, RGD) appropriate for the formation of cell-scaffold complexes. Additionally, organic polymers typically are degradable with non-toxic degradation products and with a controllable degradation rate.

As the major organic component of the natural extracellular matrix of most vertebrate tissues, collagen is arguably the most versatile substrate for supporting cell proliferation and differentiation. While more than 20 genetically distinct collagen types exist, type I collagen is the predominant form found as the major structural component of the ECM in a wide variety of tissues. The low antigenicity and immunogenicity of collagen, with adverse immune responses occurring even less frequently than nickel or latex allergies [44], make it an attractive component of tissue engineering scaffolds. Additionally, the mechanical properties and degradation rate of collagen can be tailored by altering the degree to which it is crosslinked. Furthermore, the abundance of functional groups along its polypeptide backbone makes it highly receptive to the binding of genes, growth factors and other biological molecules.

Proteoglycans are another class of organic polymers that are found in cells and that are a major component of the natural ECM. Glycosaminoglycans (GAGs) are long, unbranched polysaccharides that are a significant component of proteoglycans, do not elicit an immune response on their own, and have been used extensively for tissue engineering applications. Copolymerization of collagen with GAGs has been observed to increase the stiffness and toughness and decrease the degradation rate of collagen [45]. While the precise mechanisms leading to these effects have yet to be elucidated, collagen copolymerization with GAG is used as an alternative to heavy crosslinking of collagen which can often render the material brittle. Scaffolds fabricated from type I collagen and a glycosaminoglycan have been used to study cell migration and contraction *in vitro* [14,46,47] as well as induce regeneration of the skin, conjunctiva, and peripheral nerves *in vivo* [1,6,48,49].

1.4. Naturally derived ECM

A subgroup of organic polymer scaffolds is the naturally derived ECM. Instead of relying on technologies to fabricate a three-dimensional scaffold structure from either synthetic or natural materials, native tissue can be processed and decellularized, resulting in a biologically derived scaffold. Examples of naturally derived ECMs include the small intestinal submucosa (SIS) construct and the naturally derived collagen matrix (NDCM). Both are decellularized ECMs that have been widely used for *in vivo* tissue regeneration studies; the NDCM has been primarily used for dermal regeneration applications [50] while the SIS has been studied for urinary bladder, urethra, ureter, intestine, diaphragm, rotator cuff, and integument regeneration applications [51].

1.5. Inorganic–organic hybrid materials

In addition to the wide variety of ECM analogs derived from organic and inorganic materials, recent investigations have also attempted to produce hybrid ECM analogs with an inorganic and organic component in order to satisfy particular functional (often mechanical) requirements. Considerable interest has been generated in collagen-CaP biocomposites for their potential to mimic the composition, structure, and mechanical properties of bone. Typically, collagen-CaP composites have been produced from mechanical mixtures of pre-synthesized CaP particles suspended in a collagenous matrix [52–56] or via co-precipitation approaches [57–59]. Other Inorganic–organic hybrid materials include collagen-apatite-silicon materials to promote osseointegration during bone tissue engineering [60], calcium–silicon–poly(vinyl alcohol) hybrids for *in vitro* bone tissue engineering applications [61], and polydimethylsiloxane–tetraethoxysilane biocomposites for radial flow bioreactor studies [62]. Development and application collagen-GAG-CaP hybrids for bone and osteochondral tissue engineering applications will be described later in this text.

In this review, we summarize the development and use of collagen-glycosaminoglycan (CG) scaffolds for a variety of *in vivo* and *in vitro* applications. We first describe the fabrication of CG scaffolds with distinct chemical compositions, pore microstructures, and mechanical properties, the microstructural and mechanical characterization of these scaffolds, and cellular solids modeling tools that have been developed as a theoretical framework to describe these porous biomaterials. We then discuss *in vivo* applications of CG scaffolds, specifically their application as analogs of the extracellular matrix used as *in vivo* regeneration templates for acute and chronic injuries to the dermis, peripheral nerves, and some orthopedic tissues. Mineralized collagen-GAG scaffolds for regeneration of bone and bilayer mineralized and unmineralized collagen scaffolds for the regeneration of osteochondral defects are also described. We conclude with a discussion of the use of CG scaffolds for *in vitro* tissue engineering applications, specifically studies of cell attachment, gene expression, individual and cooperative cell contraction, and cell motility.

2. Fabrication, structure, and characterization

2.1. Fabrication via freeze drying

CG scaffolds are primarily manufactured using a freeze drying, or lyophilization, process from a suspension consisting of co-precipitated collagen and chondroitin 6-sulfate in a solution of acetic acid [1]. In short, the CG suspension is solidified at a specified freezing temperature [63], resulting in a continuous, interpenetrating network of ice crystals surrounded by the CG co-precipitate. Sublimation of the ice crystals produces the highly porous scaffold structure that is defined by individual fibers of CG, termed struts (Fig. 1). These scaffolds resemble low-density, open-cell foams, with an interconnected network of struts and relative densities typically less than 10%. Modifying CG suspension solidification allows fabrication of CG scaffolds with distinct pore microstructures. We have recently developed improved fabrication methods to produce a series of CG scaffolds with experimentally controllable pore size, but each with a uniform, equiaxed pore structure [2,63]. These scaffolds have been engineered such that well-defined microstructural environments can be presented to individual cells within the scaffold. Termed the constant cooling rate technique, a constant starting temperature of 20 °C paired with final freezing temperatures of −10, −20, −30 and −40 °C along with homogeneous suspension cooling were used to produce scaffolds of four different mean pore sizes (96–151 μm) but constant relative density ($\rho^*/\rho_s = 0.006$) (Table 1) [2]. These scaffolds have been demonstrated to possess a uniform pore microstructure with interconnected pores, and with no observed variation in pore size in orthogonal directions across the entire scaffold, suggesting an approximately equiaxed average pore [2,63]. An isothermal coarsening model has been implemented that accurately predicts CG suspension ice crystal size (and hence scaffold mean pore size) based upon the local solidification time of the suspension [64].

2.2. Peripheral nerve and spinning scaffold fabrication

Specific modifications of scaffold microstructure can be made through thermal processing for particular applications. Studies of peripheral nerve regeneration in particular have led to the fabrication of tubular CG scaffolds as well as CG scaffold plugs to insert within a tubular implant in order to reconnected transected ends of a nerve (more extensive description of peripheral nerve regeneration and CG scaffolds will be addressed later in the *In vivo* Applications section of this article). Tubular CG scaffolds for nerve regeneration are traditionally fabricated using a tubular mold and mandrel, resulting in scaffolds with a regular distribution of pores and pore sizes throughout the tube wall [49,65–67]. More recently, a spinning method has been developed for the production of tubular CG scaffolds [68]. Here the CG suspension is spun in a cylindrical copper mold about its longitudinal axis resulting in variable relative sedimentation of the CG content toward the mold outer edge; the spinning mold is then placed into a bath of liquid nitrogen. Due to the rapid solidification that results, the CG

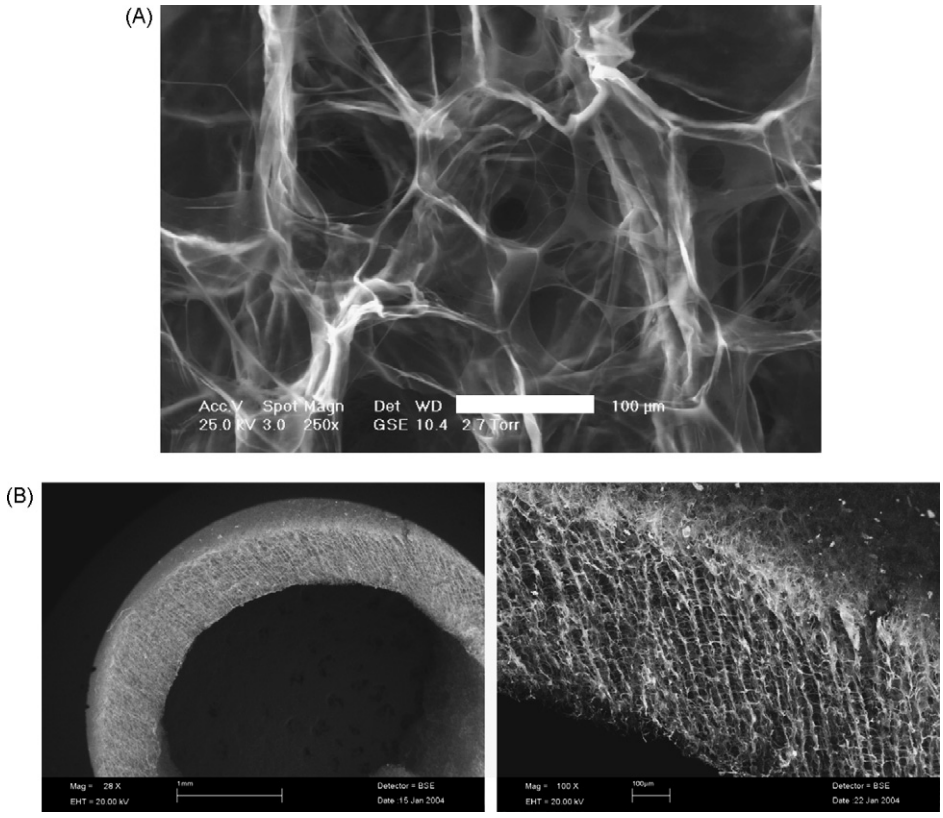

Fig. 1. (A) ESEM image of the pore structure of the CG scaffold ($T_f = -40\,^{\circ}C$). Scale bar: 100 μm. Reprinted with permission [130]. (B) SEM image of the pore structure of the tubular CG scaffold fabricated via spinning. Scale bars: 1 mm (tube), 100 μm (wall). Reprinted with permission [68,130].

content remains sedimented after the solidification and sublimation steps. The tube walls of these scaffolds display a radially aligned pore structure and a gradient of porosity along the tube radius (Fig. 1).

2.3. Mineralized and osteochondral scaffold fabrication

Specific modifications of scaffold chemical composition can also be incorporated to produce CG scaffolds for specific applications via variable mixing and thermal processing steps. Due to their composition and mechanical properties, CG scaffolds are typically used for soft tissue applications; addition of a mineral phase and incorporating variable microstructural properties throughout the scaffold have allowed a class of CG scaffolds to be developed for bone and osteochondral tissue engineering applications.

The traditional chemical composition of the CG suspension is augmented with calcium phosphate using a titrant-free, concurrent mapping technique [41,69,70]. The concurrent mapping technique allows the mineral:organic ratio (calcium phosphate mass fraction) of the collagen-GAG-CaP (CGCaP) triple co-precipitates to be varied from 0 to 80 wt%, a range that includes the mineral content of natural (cortical) bone (75 wt% CaP) [41,70]. When combined with established methods for fabricating unmineralized CG (0 wt% CaP) scaffolds [6], a series of CGCaP scaffolds can be fabricated whose composition mimics the compositions of a wide range of natural orthopedic tissue (heavily mineralized bone, non-mineralized cartilage, lightly mineralized tidemark region). The triple co-precipitate solution is freeze dried to produce a CGCaP scaffold with a homogeneous microstructure ($85 \pm 3\%$ porous), highly interconnected pores, uniform distribution of mineral content throughout the scaffold, and a controllable mean pore microstructure (mean pore sizes: 56 ± 19 to 1085 ± 83 μm) (Fig. 2) [69]. Once freeze dried, the CaP phase chemistry within the CGCaP scaffold (initially brushite) can be controlled via a hydrolytic conversion to either octacalcium phosphate or apatite, two biologically relevant CaP phases [69]. The resultant family of tissue regeneration scaffolds combines the desirable biochemical properties and pore architecture of porous CG scaffolds with the three-dimensional rigidity and direct bone-bonding properties of calcium phosphate materials in a manner that can be tailored to meet the demands of a range of applications in orthopedics and regenerative medicine.

A recent application of mineralized CG scaffolds for orthopedic applications involves production of multi-phase scaffolds

Table 1
Mean pore size and relative density of the CG scaffold variants

T_f (°C)	Mean pore size (μm) Mean ± S.D.	Relative density Mean ± S.D.
−10	151 ± 32	0.0062 ± 0.0005
−20	121 ± 23	0.0061 ± 0.0003
−30	110 ± 18	0.0059 ± 0.0003
−40	96 ± 12	0.0058 ± 0.0003

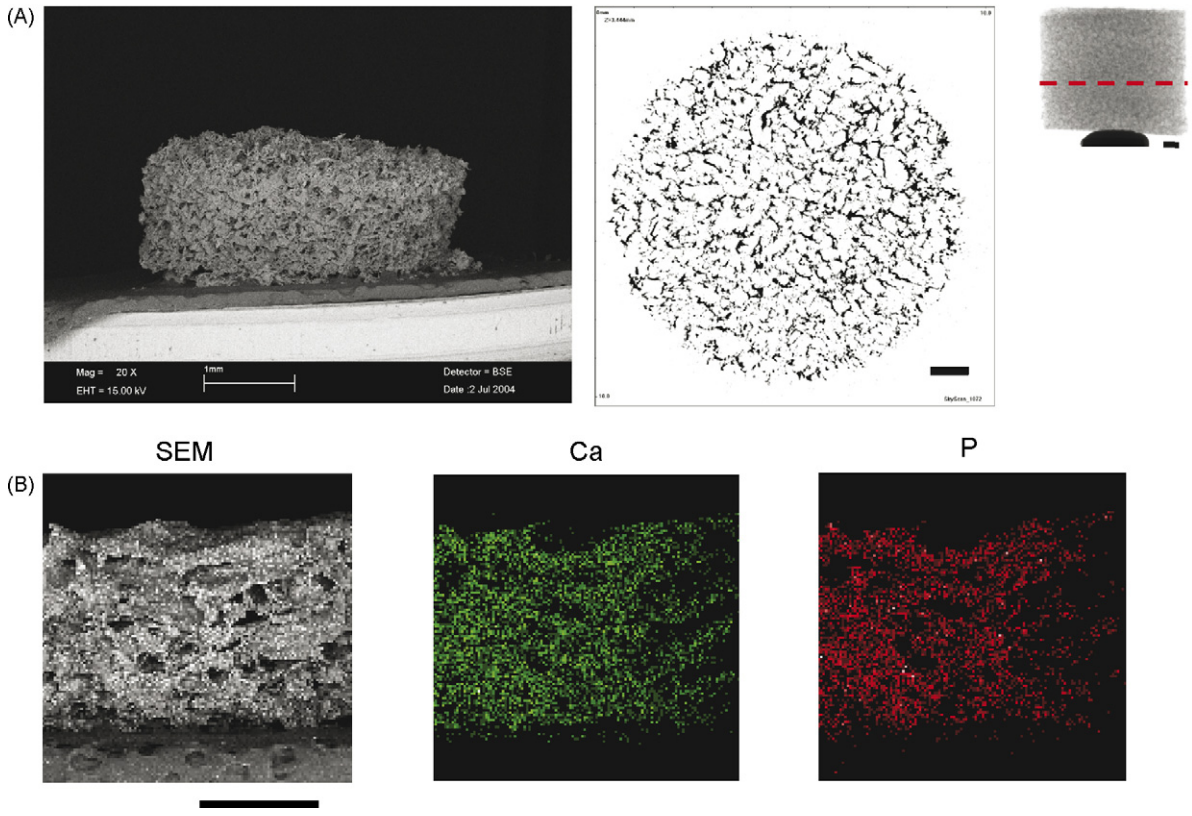

Fig. 2. (A) SEM and microCT micrographs of the gross CGCaP scaffold morphology showing an open pore structure with interconnected pores. (B) EDX analysis of CGCaP scaffold shows an even distribution of both calcium (Ca) and phosphorous (P) throughout the CGCaP scaffold. Scale bars: 1 mm. Reprinted with permission [69].

with compartments that have distinct chemical composition and pore microstructural features, but which lack hard interfaces between these compartments. A "liquid-phase co-synthesis" method enables the production of porous, layered scaffolds that mimic the composition and structure of articular cartilage on one side, subchondral bone on the other side, and – most significantly – the smooth, seamless ("soft") interface between these two tissue types found at the tidemark of articular joints [71,72]. The differential chemical composition, pore microstructure, and elastic moduli of the osseous and cartilaginous compartments enable these layered scaffolds to exhibit compressive deformation behavior that mimics behavior observed in natural articular joints [72]. Currently, these CGCaP and layered scaffolds are undergoing extensive *in vitro* and *in vivo* testing for a number of orthopedic tissue engineering applications.

2.4. Crosslinking

Crosslinking increases the mechanical strength and decreases the degradation rate of the collagen-based (CG, CGCaP, tubular) scaffolds regardless and independent of the chemical composition or pore microstructure [49,73,74]. While many crosslinking mechanisms are possible using collagen-based materials, the two most prevalent crosslinking techniques are a physical, dehydrothermal-based (DHT) process and a chemical, carbodiimide-based (EDAC) process. Both have been used extensively for *in vitro* and *in vivo* applications. Details of these crosslinking techniques and their applications have been previously described by these authors [74].

2.5. Microstructural analysis and modeling

The constant cooling rate approach allows the reproducible fabrication of a series of CG scaffolds, each with a uniform pore microstructure, constant relative density ($\rho^*/\rho_s = 0.006$), and pore interconnectivity (>99%), but variable mean pore size (96, 110, 121, 151 μm). These standardized scaffolds have undergone intensive microstructural and mechanical characterization and have facilitated development of modeling approaches to more completely describe the local microenvironment of individual cells within these scaffolds. Microstructural characterization of CG scaffolds have used conventional stereology techniques to measure scaffold pore size and the dimensions of individual struts within the scaffold microstructure as well as microCT analysis to measure scaffold mean pore size and pore interconnectivity [2,63,75].

The complex geometry of foams (and scaffolds) is difficult to model exactly; instead, dimensional arguments can be used to model salient microstructural features without incorporating exact cell geometries using the cellular solids modeling framework [76]. The first microstructural feature that was modeled using this framework was the scaffold specific surface area: the

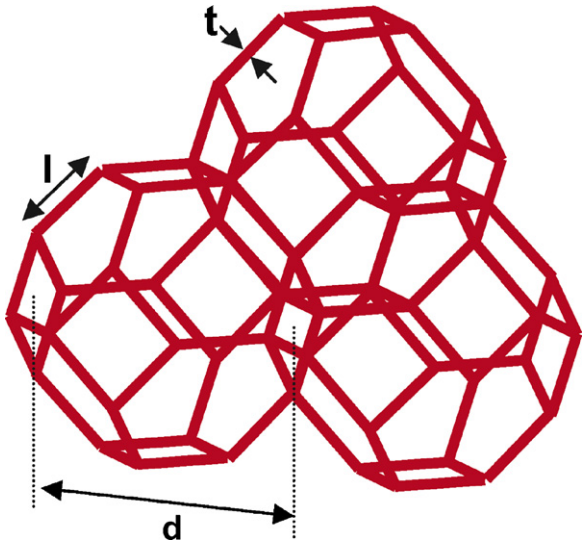

Fig. 3. Tetrakaidecahedral unit cell. *d*: pore diameter; *l*: strut length; *t*: strut thickness. Reprinted with permission [82].

total surface area of the scaffold divided by the volume of the scaffold (SA/V). SA/V describes the relative amount of surface available for cells to bind onto, and has been noted to be a critical component in defining overall scaffold bioactivity [2]. Modeling microstructural features of CG scaffolds such as SA/V is possible because the pore structure of a variety of low-density, open-cell foams has been observed to have a number of consistent features [76,77]: an approximate average of 14 faces per unit cell, 5.1 edges per face, and vertices that are nearly tetrahedral. The tetrakaidecahedron is a polyhedron that packs to fill space, approximates the structural features of many experimentally characterized low-density, open-cell foams, nearly satisfies the minimum surface energy condition, and is often used for modeling such foams (Fig. 3) [76,78]. In addition, the value of the dimensionless measure of total edge length per (unit volume)$^{1/3}$ for the tetrakaidecahedral unit cell is nearly identical to that observed for many random cellular structures [79], suggesting that the tetrakaidecahedral unit cell gives a good representation of the total edge length and can be used to model features related to the strut geometry (*i.e.*, SA/V, permeability, strut flexural rigidity) of random cellular structures such as CG scaffolds and many other tissue engineering scaffolds. For an open-cell foam with an interconnected pore structure and edges of circular cross-section modeled using a polyhedral unit cell, SA/V is related to the mean pore size (d) and the relative density (ρ^*/ρ_s, the density of the porous foam relative to that of the solid it is made from) [2,76]:

$$\frac{SA}{V} = \frac{3.65}{l}\left(\frac{\rho^*}{\rho_s}\right)^{1/2} \quad (1)$$

2.6. Permeability analysis and modeling

The permeability of scaffolds used for tissue engineering applications is important as it controls the diffusion of nutrients and waste in and out of the scaffold as well as influencing fluid pressure fields within the construct. The permeability of CG scaffolds has been determined as a function of pore size and compressive strain using both experimental and cellular solids modeling techniques. The permeability of low porosity foams (<90%), where a number of geometric factors such as porosity, tortuosity (pore interconnectivity), pore size and orientation, fenestration size and shape, and SA/V all can influence permeability, has previously been modeled and measured experimentally [80]. In these cases, construct SA/V influences permeability through frictional effects that disturb and impede fluid flow through the construct. However, such models are not applicable to highly porous materials (porosities greater than 90%) such as CG scaffolds (porosity > 99%) as well as most other tissue engineering scaffolds. An experimental device was constructed to measure the permeability of CG scaffold variants (mean pore size: 96–151 μm) at different levels of compressive strain (0, 14, 29, and 40%). Additionally, a low-density, open-cell foam cellular solids model utilizing a tetrakaidecahedral unit cell was developed to accurately model the permeability of each scaffold variant at all levels of applied strain. This model describes the permeability (k) of the CG scaffolds in terms of the scaffold mean pore size (d), percent compression (applied strain: ε), relative density (ρ^*/ρ_s), and a dimensionless system constant (A') [81]:

$$k = A'\left(\frac{d}{2.785}\right)^2(1-\varepsilon)^2\left(1-\frac{\rho^*}{\rho_s}\right)^{3/2} \quad (2)$$

The results of both the experimental and the mathematical analysis revealed that scaffold permeability increases with increasing pore size and decreases with increasing compressive strain (Fig. 4). The excellent comparison between experimentally measured and predicted scaffold permeability suggests that cellular solids modeling techniques can be utilized to predict scaffold permeability under a variety of physiological loading conditions as well as to predict the permeability of future scaffolds with a wide variety of pore microstructures.

2.7. Mechanical characterization and modeling

Scaffold mechanical properties (Young's modulus) have previously been shown to significantly influence cell behaviors such as adhesion, growth and differentiation *in vitro* as well as influence *in vivo* scaffold bioactivity [1,7–16]. The rapidly increasing use of scaffolds requires better understanding of the significant role scaffold mechanical properties play in influencing cell behavior and overall scaffold bioactivity. To develop a standardized and well-characterized series of constructs for *in vitro* applications, the tensile and compressive behavior of CG scaffolds fabricated using the constant cooling rate approach (uniform pore microstructure; ρ^*/ρ_s: 0.006; Mean pore sizes: 96–151 μm) [2,63], as well as the elastic modulus of the individual struts that define the scaffold network has been evaluated.

In addition to experimental characterization, cellular solids modeling has again been incorporated to analyze the relationship between scaffold microstructure and mechanical properties. The stress–strain curve for a low-density, elastomeric open-cell foam (such as the CG scaffold) in compression is characterized

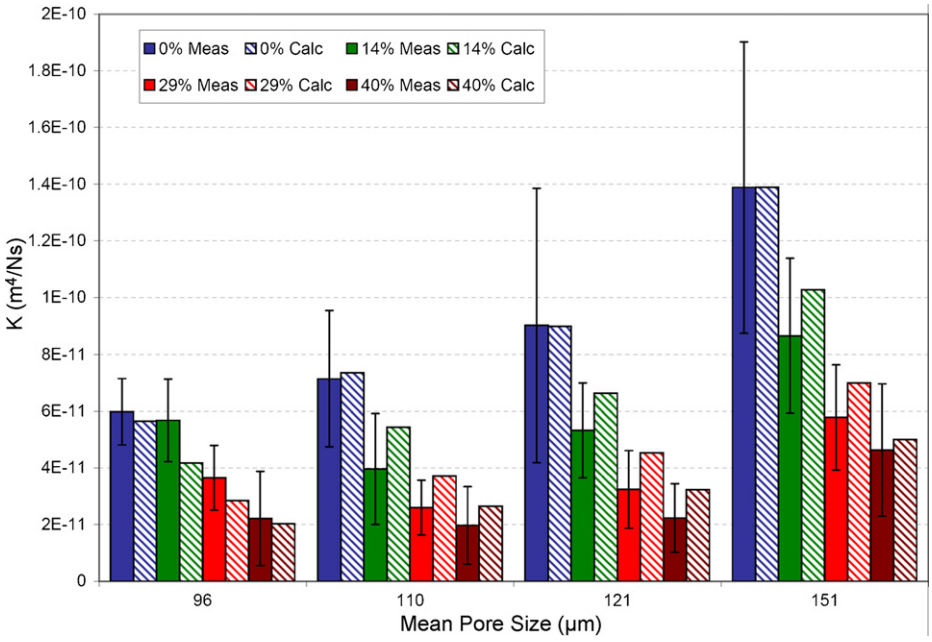

Fig. 4. Comparison between the experimental results (K_{meas}, solid bars) obtained and the predicted values obtained from the mathematical model (K_{calc}, striped bars) for CG scaffold permeability (fluid mobility) under varying compressive strains (0, 14, 29, 40% strain, left to right for each pore size) for distinct pore sizes (96, 110, 121, 151 μm). Reprinted with permission [81].

by three distinct regimes: a *linear elastic regime* (controlled by strut bending), a *collapse plateau regime* (struts buckling and pore collapse), and a *densification regime* (complete pore collapse throughout the material) (Fig. 5) [76]. In tension, the initial linear elastic response is typically the same as is observed in compression for small strains. However, as the strain increases, the struts become increasingly oriented in the direction of applied tension, increasing the stiffness until tensile failure occurs.

The Young's modulus (E^*) and elastic compressive strength (σ^*_{el}, also called the compressive plateau stress) of elastomeric open-cell foams such as tissue engineering scaffolds depend on the foam relative density, ρ^*/ρ_s, the Young's modulus of the solid from which the foam is made, E_s (termed the strut modulus), and a constant related to the cell geometry. The complex geometry of foams (and scaffolds) is difficult to model exactly; instead, dimensional arguments were used that rely on modeling the mechanisms of deformation and failure in the foam (edge bending and buckling), but not the exact cell geometry [76]. For elastomeric cellular solids, E^* and σ^*_{el} are:

$$E^* = C_1 \left(\frac{\rho^*}{\rho_s}\right)^2 E_s \tag{3}$$

$$\sigma^*_{el} = C_2 \left(\frac{\rho^*}{\rho_s}\right)^2 E_s \tag{4}$$

C_1 and C_2 are constants of proportionality related to the cell geometry. Data for a wide variety of open-cell foams indicate that $C_1 \sim 1$ and $C_2 \sim 0.05$ [76]. Both the Young's modulus (E^*) and the compressive strength (σ^*_{el}) of elastomeric open-cell foams vary with the square of the relative density so that the strain at which cell collapse by buckling occurs, ε^*_{el}, is constant, independent of E_s or ρ^*/ρ_s, and equal to $C_2/C_1 = 0.05$. Both E^* and σ^*_{el} are expected to be independent of the cell or pore size [76].

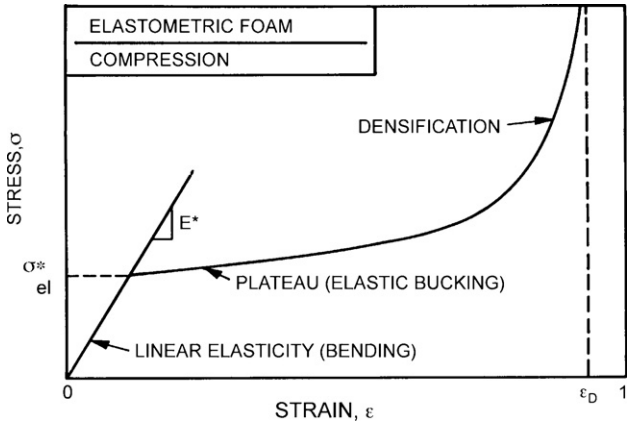

Fig. 5. Schematic uniaxial stress–strain curve for an elastomeric cellular solid in compression showing linear elastic, collapse plateau, and densification regimes as well as the linear elastic modulus (E^*) and elastic collapse stress (σ^*_{el}). Reprinted with permission [76].

Experimentally, the CG scaffold variants exhibited stress–strain behavior characteristic of low-density, open-cell foams with distinct linear elastic, collapse plateau, and densification regimes (Fig. 6). The scaffolds with equiaxed pores were found to be mechanically isotropic. The independent effects of hydration level, pore size, crosslink density, and relative density on the mechanical properties was also determined (Tables 2 and 3) [74]. Further independent control over scaffold Young's modulus (via post-fabrication crosslinking independent of scaffold microstructure) and microstructure (scaffold pore size independent of Young's Modulus) was

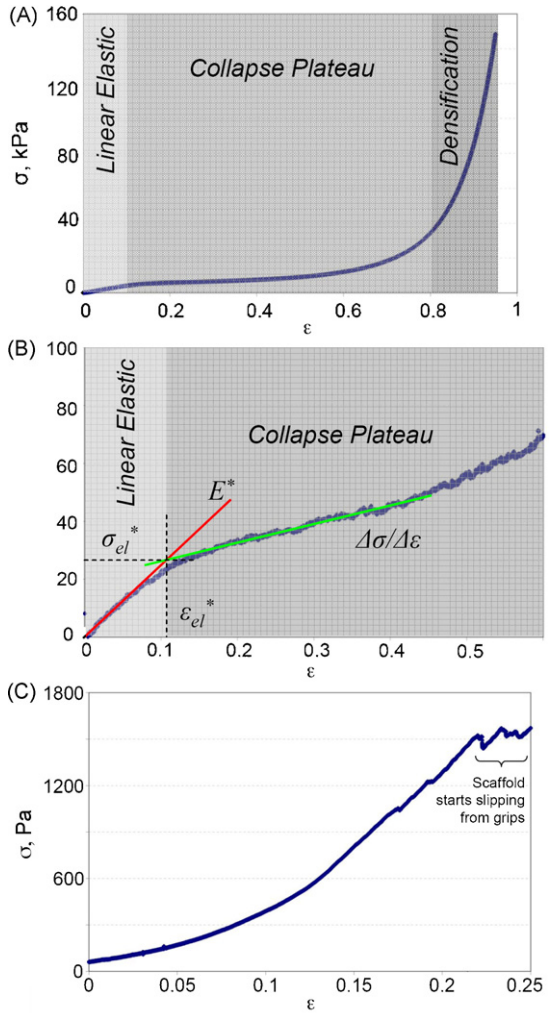

Fig. 6. Characteristic stress–strain curves observed for the CG scaffold under compression for the entire tested strain range (A) ε: 0–0.95, and for a subregion of a hydrated CG scaffold (B) ε: 0–0.60. Linear regressions of the linear elastic and collapse plateau regimes are used to calculate the linear elastic modulus (E^*) and the collapse plateau modulus ($\Delta\sigma/\Delta\varepsilon$).The elastic collapse stress and strain are σ^*_{el}, ε^*_{el}. (C) Characteristic stress–strain curve observed for the (hydrated) CG scaffold variants under uniaxial tensile testing in the plane of the scaffold sheet. Complete mechanical characterization results are displayed in Tables 2 and 3. Reprinted with permission [74].

observed. The Young's modulus (E_s) of the individual scaffold struts that define the scaffold microstructure was measured via AFM (Fig. 7) [74]. Good agreement was observed between experimental results of scaffold mechanical characterization

Table 2
Average (Mean ± S.D.) mechanical properties of the homogeneous CG scaffold variants (96–151 μm; 0.006 relative density; DHT crosslinking at 105 °C for 24 h; hydrated)

Property	Hydrated CG Scaffold
E^*	208 ± 41 Pa
σ^*_{el}	21 ± 8 Pa
ε^*_{el}	0.10 ± 0.04
$\Delta\sigma/\Delta\varepsilon$	92 ± 14 Pa
E_s	5.28 ± 0.25 MPa

Table 3
Elastic moduli of individual scaffold struts within hydrated CG scaffolds crosslinked via DHT and EDAC/NHS techniques [74]

Crosslinking treatment	Scaffold strut elastic moduli (MPa) Mean ± S.D.	Relative elastic modulus
Uncrosslinked	3.9 ± 0.20	0.74
DHT105/24 (Standard)	5.28 ± 0.25	1.0
DHT120/48	5.7 ± 0.30	1.08
EDAC1:1:5	10.6 ± 0.50	2.0
EDAC5:2:5	11.8 ± 0.56	2.24
EDAC5:2:1	38.0 ± 1.8	7.2

and low-density, open-cell foam model predictions for the scaffold E^* and σ^*_{el} (Eqs. (3) and (4)) for the standard CG scaffold variants (ρ^*/ρ_s: 0.006; mean pore size: 96–151 μm). While the open-cell foam model correctly predicted the relationship between E_s and E^* for the series of CG scaffolds with a uniform pore microstructure, it over-predicted the measured moduli (E^*) at higher ρ^*/ρ_s, likely due to regions of microstructural heterogeneities observed in these higher density scaffolds [74].

Besides further validating the use of cellular solids theory to describe the materials and mechanical properties of this CG scaffold system, the most significant aspect of this investigation was that a homologous series of experimental substrates have been fabricated and then structurally (mean pore size, SA/V, permeability) and mechanically characterized. These scaffolds represent a series of well-defined biomaterials appropriate for quantitative experimental assays where the local microstructural and mechanical properties of the extracellular environment surrounding individual cells within these scaffolds can be defined and modified in discrete increments. These characterized scaffold variants provide a standardized framework for a series of quantitative *in vitro* and *in vivo* tissue engineering studies, notably an investigation of the independent and synergistic effect

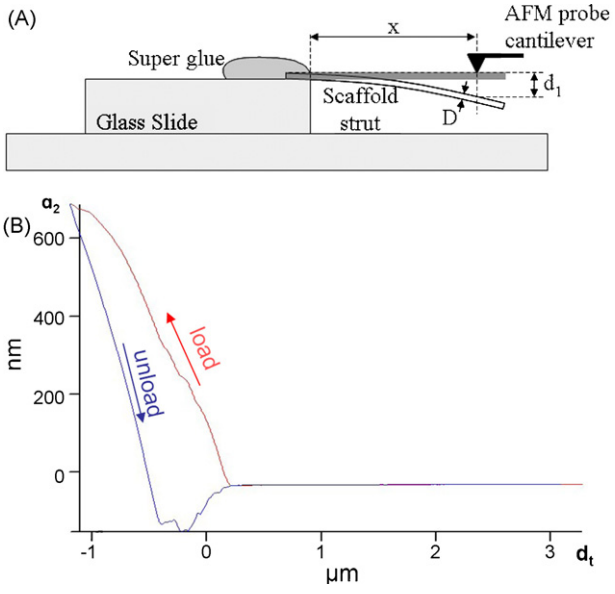

Fig. 7. (A) Experimental arrangement to perform bending tests on individual CG scaffold struts. (B) Characteristic load–unload curve for bending tests performed via AFM on individual CG scaffold struts. Reprinted with permission [74].

of the mechanics and microstructure of a 3D substrate on cell migration and contraction [82] described later in this review, and further development of scaffolds appropriate for mesenchymal stem cell [83] and orthopedic applications [69].

3. *In vivo* applications

A primary use of CG scaffolds has been to induce regeneration of tissues following severe injury [1]. The typical mammalian physiological reaction to both chronic and acute severe injuries is characterized by a complex inflammatory response, cell-mediated wound contraction, and scar tissue synthesis termed *repair*. However, introduction of a suitable analog of the ECM into the wound site has been observed to block cell-mediated contraction of the wound site and induce *regeneration* of physiological tissue. Although several ECM analogs have been studied, only those with a narrowly defined structure, specifically some CG scaffold variants, have been shown to be capable of regeneration. The microstructural, chemical compositional, and biodegradation rate specificity of these CG scaffolds appears to be related to the requirement for inhibition of wound contraction prior to the incidence of regeneration.

3.1. CG scaffolds for dermal regeneration

The dermal regeneration template (DRT) is a CG scaffold whose microstructural and materials properties have been optimized to produce a bioactive ECM analog that, when implanted, induces sequential regeneration of the underlying dermis and resultant regeneration of the basement membrane and epithelial layers of the skin. The DRT is fabricated from CG copolymer with a 98:2 ratio of microfibrillar, type I collagen to chondroitin 6-sulfate. The microstructure of the DRT has been optimized with both a lower and upper pore size bound of 20 ± 4 and 125 ± 35 μm, respectively. The biodegradation rate of the DRT has been optimized with lower and upper bounds of residence time in the wound bed of 5 and 15 days, respectively [1,6].

The DRT is typically used as an acellular implant that induces regeneration of the dermis, thereby providing the essential substrate for spontaneous regeneration of the epidermis and basement membrane layers. Following dermal regeneration by the unseeded DRT, epidermal cells from the wound edges migrate into the center of the wound and form a mature epidermis and basement membrane in a process termed sequential regeneration [1]. The resultant regeneration of appropriate tissue layers (tissue triad) along with associated structures (*i.e.*, rete ridges) has indicated that the DRT is capable of inducing regeneration of mature skin in a full-thickness skin wound model [84]. The effectiveness of the DRT has been demonstrated clinically with a population of massively burned patients [1] and in animal experiments utilizing a full-thickness (anatomically well defined skin wound) skin wound [1,6].

3.2. CG scaffolds for peripheral nerve regeneration

The anatomy of peripheral nerve injuries requires a multipart implant for *in vivo* regeneration applications: a tubular scaffold used to reconnect the transected nerve stumps and a second material that is placed within the lumen of the tube which enhances the quality of peripheral nerve regeneration. Collagen-based scaffolds play a role in both parts of this combination. Peripheral nerve regeneration is not observed in the absence of a tubular device if the gap between the two transected stumps is greater than a few millimeters [85]. While it has been observed that a tube is sufficient to induce regeneration across a gap of modest length following complete transection, the physical parameters of the tube and any material in the tube lumen significantly affect the kinetics and quality of regeneration [1].

Conduits (tubes) fabricated from ECM components, specifically collagen, fibronectin, and laminin, have been generally shown to enhance the quality of peripheral nerve regeneration. Type I collagen tubes in particular have been observed to induce the highest quality of regeneration, as defined by both morphological and electrophysiological methods [1,85]. Protein and cell permeable tubes exhibited significantly superior quality of peripheral nerve regeneration and significantly reduced wound contraction and scar synthesis compared to protein-permeable, cell-impermeable as well as non-permeable tubes [1,85]. The quality of peripheral nerve regeneration was observed to vary significantly with tube degradation rate as well, with the highest quality of regeneration observed for tubes with a degradation half-life ($t_{1/2}$) of 2–3 weeks (Fig. 8) [49].

A wide variety of solutions, ECM analogs, and cell suspensions have been introduced into the tube lumen in an effort to improve the quality of peripheral nerve regeneration. Use of ECM macromolecules in the form of solutions or gels has no significant effect on peripheral nerve regeneration; however, an insoluble structure (scaffold) within the tube lumen leads to the highest quality of regeneration [85]. The ECM analog that induces the highest quality of regeneration is the Nerve Regeneration Template (NRT) [1,86]. The NRT is fabricated from CG copolymer with a 98:2 ratio of microfibrillar, type I collagen to chondroitin 6-sulfate. Like the DRT, the pore structure of the NRT significantly influences its effectiveness. Unlike the homogeneous pore microstructure of the DRT, the NRT is fabricated with axially (extending between the proximal and distal stumps) elongated pore tracks defined by axially oriented ellipsoidal pores with pore sizes of order 10–20 μm that provide directional guidance to the formation of linear Schwann cell columns between the transected nerve stumps which act as tracks for eventual axon elongation [1]. The degradation rate of the NRT significantly affects the quality of regeneration, with a half-life of degradation on the order of 6 weeks found to be optimal [1,86]. The long-term morphological structure and electrophysiological function of nerves regenerated using the NRT has been observed to be at the level of an autografted nerve, the current gold-standard for peripheral nerve injury treatment [66,87].

3.3. CG scaffolds for cartilage, meniscus tissue engineering

CG scaffolds have been used for *in vivo* and *in vitro* studies of regeneration of a host of orthopedic materials, namely articular

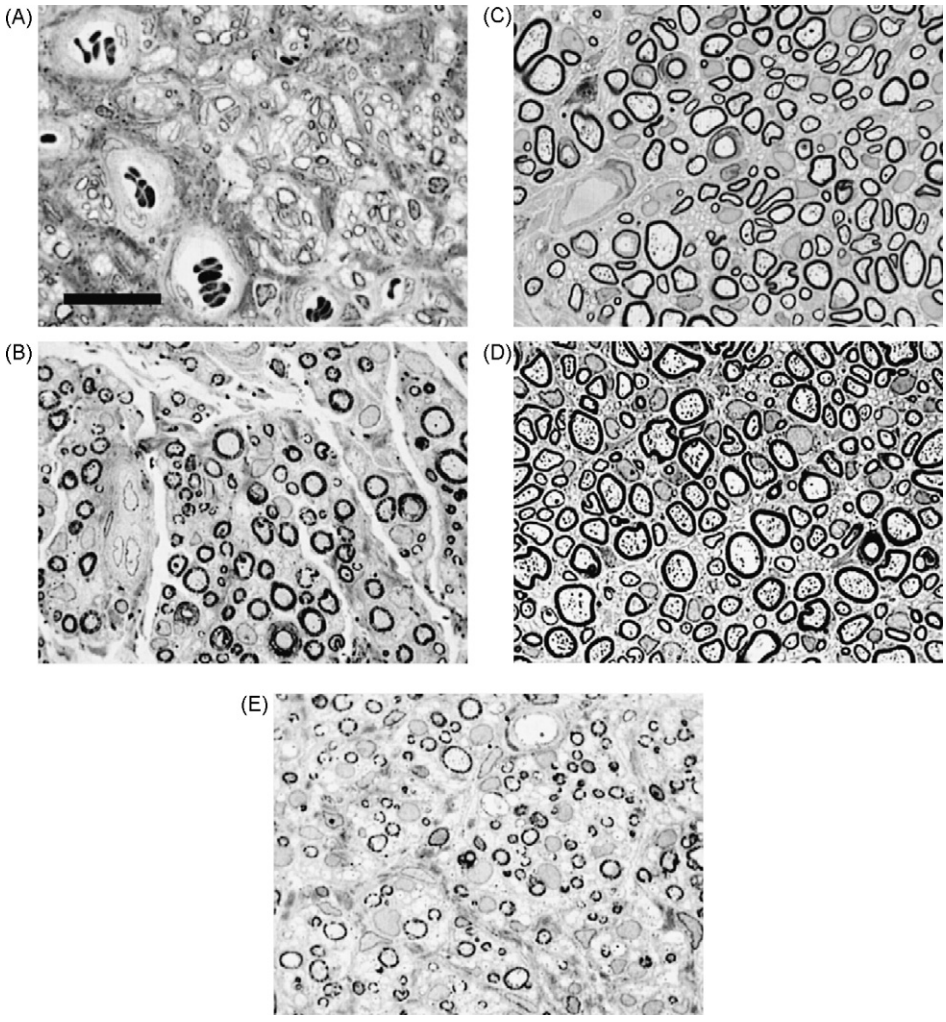

Fig. 8. Histomorphometic, cross-sectional images of the nerve trunk regenerated using collagen tubes with distinct degradation rates. The devices are arranged in order of lowest to highest crosslink density, or most rapid to slowest degradation rate from A to E. Nerves trunks regenerated in devices C and D, characterized by intermediate levels of the crosslink density and degradation rate (device half-life: 2–3 weeks), showed superior morphology, with significantly larger axons, a more well-defined myelin sheath, and a significantly larger N-ratio. Scale bar: 25 μm. Reprinted with permission [49], S. Karger AG, Basel, Switzerland.

cartilage, meniscus, and the intervertebral disk. The effect of crosslinking density, chemical composition, and pore size of CG scaffolds, as well as the use of gene- and growth factor-seeded CG scaffolds, have been studied extensively in the context of articular cartilage regeneration [88–93]. Recently, CG scaffolds have also been applied to meniscus [94] and intervertebral disk [95] tissue engineering applications, with further promise for optimization.

3.4. CGCaP scaffolds for bone, osteochondral regeneration

Single phase and layered, multi-phase CG-based scaffold have recently been developed for *in vivo* bone and osteochondral tissue engineering applications [41,42,69–72]. These CGCaP-based scaffolds were developed to mimic the compositional and structural requirements of bone and osteochondral injuries. Microstructural, chemical, and mechanical analysis of the osteochondral scaffold suggests that it possesses distinct regions characterized by differential pore microstructure, mechanical properties, and chemical composition with a soft interface between the regions that mimics that seen in the natural osteochondral region. Currently these scaffolds are undergoing extensive *in vivo* testing as stand-alone bone plugs (in the monolithic CGCaP form) and as full osteochondral scaffolds.

The family of bone regeneration scaffolds is fabricated from type I collagen, glycosaminoglycans (chondroitin 6-sulfate), and CaP. These scaffolds have been fabricated with a homogeneous, interconnected pore structure with high porosity ($85 \pm 3\%$ porous) whose pore architecture (mean pore size: 56 ± 19 to 1085 ± 83 μm), mineral content (0–80 wt% CaP), CaP phase chemistry (brushite, octacalcium phosphate, apatite), and crosslinking density can be independently controlled. Preliminary results suggests that the monolithic CGCaP scaffolds for bone tissue engineering integrate rapidly into bone defects and show preliminary bony substitution and direct bone-mineral apposition within the implant as early as 6 weeks post implantation [96].

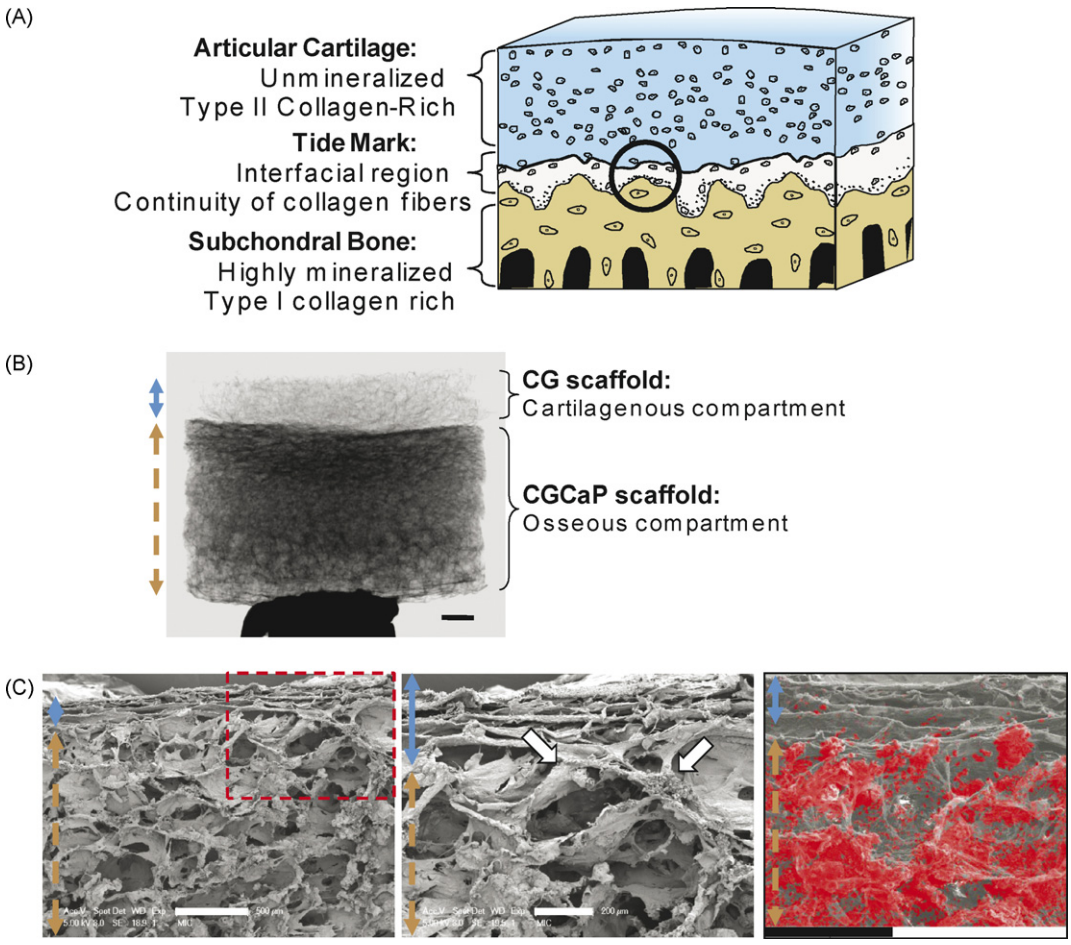

Fig. 9. (A) Structure of the articular joint. (B) X-ray microCT image of the layered osteochondral scaffold showing distinct cartilaginous and osseous compartments (scale bar 1 mm). (C) SEM micrographs of the osteochondral scaffold showing the complete scaffold microstructure (left; scale bar 500 μm), and the interfacial region (middle; scale bar 200 μm) showing continuity between the osseous (tan dashed arrow) and cartilaginous (blue solid arrow) compartments including collagen fibrils extending across the transition (white arrows). No regional areas of delamination or debonding are observed between the compartments. Distribution of Ca mineral (P similar but not shown) content (red shading) superimposed over an SEM image of the osteochondral scaffold showed distinct mineralized (high CaP content, tan dashed arrow) and unmineralized (low/zero CaP content, blue solid arrow) layers (right; black scale bar 400 μm) [72].

The family of osteochondral scaffolds is fabricated from collagen (type I and II), glycosaminoglycans (chondroitin 6-sulfate), and CaP (brushite, octacalcium phosphate, apatite). The layered design of these scaffolds mimics the composition and structure of the natural articular joint, in which mineralized (type I collagen-GAG-CaP) and unmineralized (type II collagen-GAG) layers are joined at a smooth, stable ("soft") interface (Figs. 2 and 9). The technologies and methods used to produce the scaffolds enable a number of key parameters (including CaP mass fraction, CaP phase, organic phase, pore architecture, and crosslink density) to be accurately and reproducibly controlled over ranges relevant to the *in vitro* and *in vivo* performance of biomaterials and tissue regeneration scaffolds. Under mechanical loading, the osteochondral scaffolds perform as expected for a biphasic materials, with the majority of deformation confined to the cartilagenous compartment; further, no evidence of delamination or debonding of the layers was observed during or following loading [72]. *In vivo* testing of these osteochondral scaffolds is ongoing.

4. *In vitro* applications

4.1. CG scaffolds to study cell attachment

The biological activity of scaffolds used in tissue engineering applications hypothetically depends on the density of available ligands, scaffold sites at which specific cell binding occurs. Ligand density is characterized by the composition of the scaffold, which defines the surface density of ligands, and by the specific surface area of the scaffold, which defines the total surface of the structure available to cells. The surface area per unit volume (SA/V), or specific surface area, of each scaffold was estimated using a cellular solids model utilizing a polyhedral unit cell to determine the effect of mean pore size on the CG scaffold SA/V. To study the relationship between cell attachment and viability and scaffold microstructure, the CG scaffolds with a constant composition and solid volume fraction ($\rho^*/\rho_s = 0.006$), but with four different pore sizes (96–151 μm) corresponding to four levels of specific surface area were seeded with MC3T3-E1 mouse clonal osteogenic cells [2]. The cells and scaffold

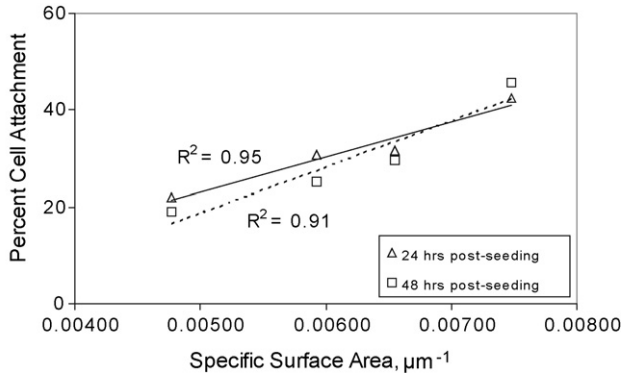

Fig. 10. Attached cell number plotted against specific surface area showing a strong linear relationship at 24 (solid line) and 48 h (dashed line) post-seeding. Reprinted with permission [2].

were maintained in culture and the number of viable cells that remained attached was counted. The results of the cell attachment/viability assay were then considered in the light of cellular solids modeling tools used to describe scaffold specific surface area. The fraction of viable cells attached to the CG scaffold decreased with increasing mean pore size, increasing linearly ($R^2 = 0.95$, 0.91 at 24 and 48 h, respectively) with the scaffold SA/V (Fig. 10). The strong correlation between CG scaffold SA/V and cell attachment indicates that cell attachment and viability are primarily influenced by scaffold specific surface area over this range (96–151 μm) of pore sizes for MC3T3 cells.

4.2. CG scaffolds to study gene expression

The CG scaffold system has been used to probe the role ECM surface topology plays in influencing gene expression profiles. Cell remodeling of its local extracellular environment and induced-angiogenesis are two critical features to study (and eventually control) for many tissue engineering applications. Gene expression profiles for genes involved in angiogenesis (*i.e.*, VEGF, HMOX, and HGF) and ECM remodeling (*i.e.*, matrix metalloproteinases, ECM components) were compared for fibroblasts cultured within CG scaffolds fabricated via a phase separation method versus fibroblasts cultures on deposited 2D CG surfaces. Differential expression of these genes was observed for cells in 3D constructs versus on 2D surfaces. Genes for some matrix metalloproteinases (*i.e.*, MMP-2, MMP-12, MMP-19), ECM component synthesis (*i.e.*, COL1A2, COL3A2, COL2A1, COL4A4, COL4A5), and pro-angiogenic factors were upregulated while some MMP inhibitors (*i.e.*, TIMP1, TIMP3) were downregulated for cells cultured in the 3D CG constructs versus on the 2D CG surfaces [97]. These results suggested that the 3D presentation of ECM components is a critical feature in stimulating differential gene expression profiles.

4.3. CG scaffolds to study cell contraction

Cell-mediated contraction plays a critical role in many physiological and pathological processes, notably organized contraction during wound healing. Improved understanding of cell contraction represents an important area of study in tissue engineering. Traditionally, studies of cell contraction *in vitro* have been performed using two-dimensional substrates. Cells are seeded onto a two-dimensional substrate or onto a semi-3D substrate such as the microfabricated post array detector (mPADs) system and the deformation of the substrate or individual posts by the cell is measured; the value of the contractile force is then determined using the modulus of the substrate [98–104]. This technique also allows correlation of substrate deformation (and force) with observed cell processes such as pseudopod extension and cell migration via microscopy techniques [99,105–107] and have shown substrate modulus significantly modifies cell behaviors such as DNA biosynthesis, differentiation, migration speed, directional persistence, and applied traction forces [13,102,103,107–115]. Using these methods, fibroblasts are estimated to be capable of generating contractile forces in the hundreds of nanoNewtons [103,104,114]. However, the fact that the shape (and likely cytoskeletal organization) of cells on two-dimensional and mPAD substrates (amorphous, spread polygonal) is significantly different than that of fibroblasts observed in wound sites, within the natural ECM, and in 3D materials such as CG scaffolds (elongated spindle-shaped) suggests that the contractile capacity of cells on/in these different substrates/constructs might be significantly different [75,116–118].

CG scaffolds have been used to study the macroscopic contractile behavior of cell populations, the contractile behavior of individual cells within the CG scaffold network, and the relationship between the cell/cytoskeletal organization and cell contraction in 3D materials. The average contractile force generated by a cell population can be calculated from the gross deformation of the CG scaffold by a known population of cells as well as the Young's modulus of the scaffold. During contraction within the CG scaffold, dermal fibroblasts are observed to undergo morphological reorganization. After seeding, initially rounded fibroblasts (diameter 20 μm) then attached to the CG scaffold and elongated over time into spindle-shaped cells. The average cell aspect ratio (maximal cell length/maximal cell thickness) increased from 1.4 to 2.8 during the first 15 h in the scaffold (Fig. 11) [119]. Scaffold deformation occurs simultaneously with this cell elongation and presumably cytoskeletal reorganization [14,119]. The force generated by a population of dermal fibroblasts within the CG scaffold tends to reach an asymptote after approximately 12 h [14]. The average cell contraction force generated by dermal fibroblasts with these CG scaffolds was calculated by measuring the gross dimensional change of the rectangular scaffold sample (58 mm × 28 mm × 3 mm) when seeded with millions of cells (2.3–10 × 10^6 cells), to be 1.4 ± 0.2 nN, independent of the number of cells seeded [14]. When the stiffness of the system was changed, fibroblasts applied differential levels of strain but a constant average force to the CG scaffold, suggesting that cells apply contractile forces independent of the local microenvironment (Fig. 11) [120]. However, two significant assumptions are made when measuring cell contraction in this manner. The dimensional changes of the rectangular scaffold sample were measured in only one direction and the fraction of contractile cells versus the total cell population within the scaffold was not

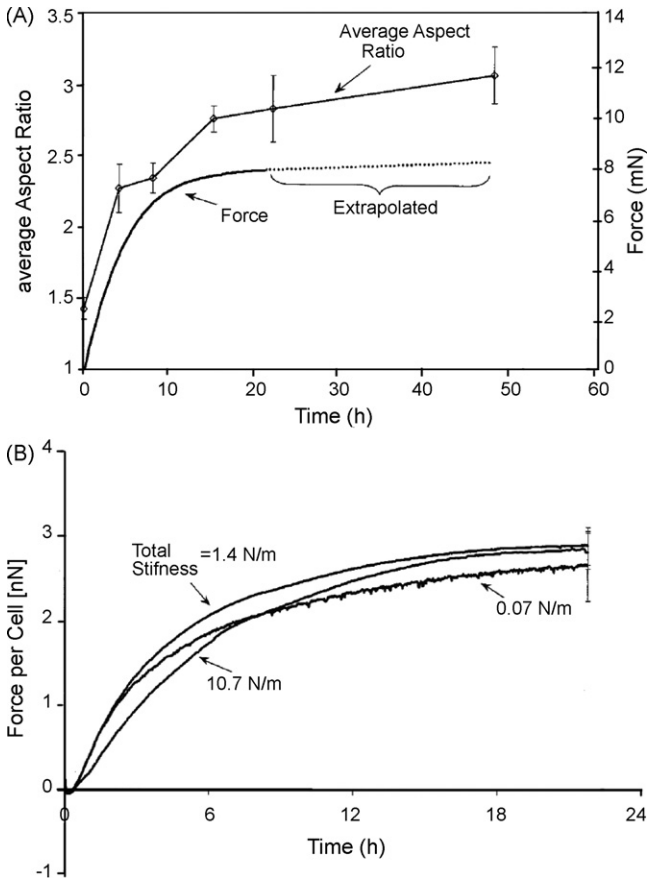

Fig. 11. (A) Plot of the fibroblast aspect ratio and generated contractile force with time in the CG scaffold. The average cell aspect ratio increased up to 15 h post-seeding in a manner similar to the total force generated by the cell population. (B) Plot of force per cell over time for different system stiffnesses. The displacement developed per cell increased as the system stiffness decreased but the force developed per cell was independent of the system stiffness. Reprinted with permission [119,120].

characterized. So, the average force per cell was calculated using the assumptions that all cells were contracting in the direction that dimensional change was measured and that all cells were contracting at the same time: $F_c = 1.4 \pm 0.2$ nN is therefore a lower bound.

CG scaffolds have also been used to study the contractile capacity of individual cells within a model 3D environment. Time-lapse images of individual cells within the scaffold can be taken using a phase contrast microscope; individual cells are observed migrating through the scaffold network or contracting the scaffold network, resulting in buckling of the strut(s) to which the cell is attached (Fig. 12) [14,119,120]. Cellular solids theory was applied with conventional column buckling relationships in order to quantify the magnitude of individual cell contraction events within the CG scaffold [75]. This technique can be used to study cell contraction and cell-scaffold interactions within a wide variety of porous scaffolds provided that they resemble low-density, open-cell foams. This method also extends previous methods for analyzing cell buckling of two-dimensional substrates to three-dimensional constructs because it allows individual cell behavioral and contraction events to be observed and quantified.

The magnitude of the cell-mediated contraction forces generated by individual dermal fibroblasts within the CG scaffold is calculated from the strut characteristics (l, d, E_s) and is termed the individual cell contraction assay [75]. This calculation utilizes detailed mechanical characterization of the CG scaffolds [74] and previous experimental and theoretical work describing the mechanics and collapse of open-cell foams [76]. The buckling load applied to an individual strut within the scaffold network was calculated by incorporating the restraining effect of the surrounding strut network in order to most appropriately model the boundary conditions of the buckling strut. When an elastomeric cellular solid is loaded such that the cell edges (*i.e.*, CG scaffold struts) are under compression, the edges first bend and then buckle [76,121]. When a cell-generated contractile force is applied to the local strut network, the strut most nearly aligned with the axis of compression buckles but is restrained at its ends by the other struts; the surrounding strut network tends to reduce the rotation of the buckling strut ends. This restoring moment per unit rotation is most closely modeled by a rotational stiffness applied at the ends of the buckling strut by the three restraining struts (Fig. 12) [76]. The effect of individual fibroblasts buckling the CG scaffold struts can be similarly described using these previously developed open-cell foam models for isotropic materials. The critical load (F_c) at which a scaffold strut of length l, average diameter d, Young's modulus E_s, and second moment of area I (strut geometry was approximated as a cylindrical fiber, $I = \pi d^4/64$) buckles can be calculated by Euler's formula and the hydrostatic compression end restraint ($n^2 = 0.34$) [75,76,121]:

$$F_c = \frac{n^2 \pi^2 E_s I}{l^2} \tag{5}$$

The contractile force generated by individual dermal fibroblasts that were able to buckle a CG scaffold strut was calculated to range between 11 and 41 nN, with an average contractile force (F_c) of 26 ± 13 nN (Mean $\pm$ S.D.) [75]. In one instance a cell was unable to buckle the strut it was attached to because that strut was significantly thicker ($\sim$10 μm versus 3.9 μm) than the average strut, thereby increasing its flexural rigidity ($E_s I$) and buckling load (F_c). The buckling load of this strut provides an upper bound of the contractile capacity of the cell. Analysis of the local strut microstructure from these images determined that this particular strut was approximately 10 μm in thickness and 130 μm in length, indicating that the force required to buckle the strut was approximately 450 nN. These results suggest that while dermal fibroblasts can easily develop the $\sim$25 nN force required to buckling conventional CG scaffold struts, fibroblasts within a fibrillar collagen network are unable to develop contractile forces at the level of 450 nN [75].

4.4. CG scaffolds to study cell motility

Cell migration is a complex process governed by many factors including extracellular ligands and intracellular signaling [122,123]. Cell motility plays critical roles in a number of such processes, notably organized wound contraction and fibroblast and vascular endothelial cell migration during wound healing

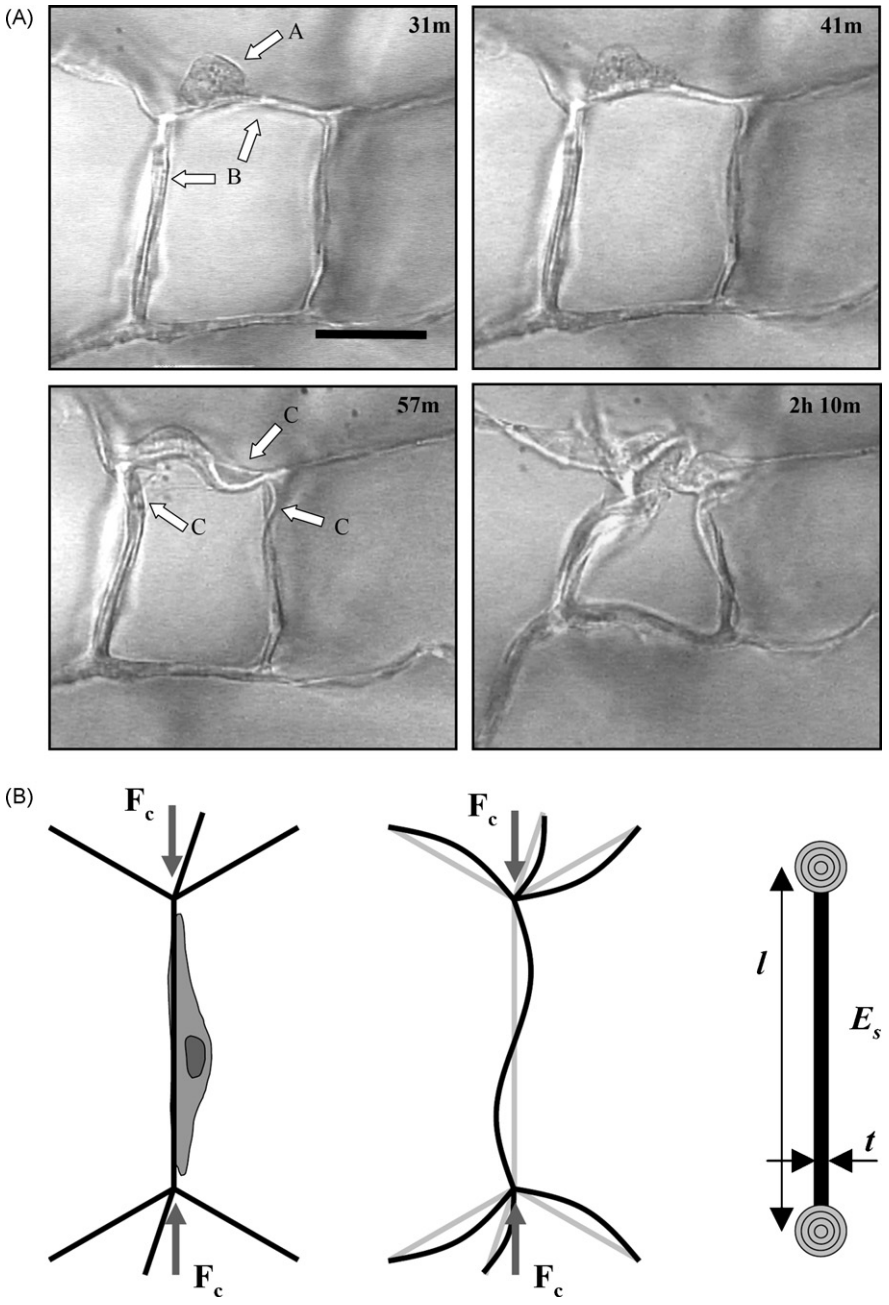

Fig. 12. (A) Time-lapse images of an individual dermal fibroblast within the CG scaffold. The sequence of images shows a dermal fibroblast (arrow A) elongating and deforming the scaffold surrounding struts (arrows B). Several struts are deformed over time (arrows C). The number in the top right corner of each image indicates the time, in hours and minutes, after cell seeding. Scale bar: 50 μm. Reprinted with permission [119]. (B) Schematic of a single cell applying a critical buckling load (F_c) to a scaffold strut within an idealized CG scaffold network (left). The surrounding struts inhibit rotation of the ends of the buckling strut (middle). A simplified model of CG scaffold strut buckling with the appropriate boundary conditions: the scaffold strut is restrained at its ends by a rotational spring that represents the surrounding strut network (right). Reprinted with permission [75,119].

[1], metastatic tumor cell migration [124], stem cell mobilization and homing [125,126], and tissue remodeling [1]. Studies of cell motility on 2D substrates have led to an improved understanding of how surface features and especially substrate stiffness affect migration through changes in cytoskeletal organization and applied traction forces [107,108,113]. While these experiments have begun to probe cell-substrate interactions on two-dimensional surfaces, understanding the critical biochemical and biophysical parameters that affect cell motility in three-dimensional constructs such as scaffolds and gels is an important new avenue of research. Cell motility into and within 3D tissue engineering constructs is a useful model system for studying cell migration relevant to both physiological and pathological conditions with applications in many areas such as tissue engineering and cancer biology. In particular, understanding extracellular influences on cell motility within physiologically relevant three-dimensional constructs can aid the design of future bioactive constructs since an initially acel-

lular scaffold must be rapidly cellularized either *in vitro* or *in vivo*.

Quantitative study of individual cell behavior within a three-dimensional scaffold construct requires understanding the local extracellular environment of the individual cells through accurate compositional, microstructural, and mechanical characterization. The series of CG scaffolds with uniform, well-characterized, and independently controllable mechanical and microstructural properties are an ideal platform for *in vitro* studies of the effect of the extracellular matrix environment on cell behavior. The CG scaffold pore sizes are significantly larger than the characteristic dimension of the fibroblasts; hence, cells are not exposed to steric hindrance as in a dense network of thin ECM fibers. Rather, cells are forced to migrate along scaffold struts, a phenomenon known as contact guidance. To specifically address the question of how scaffold pore size affects cell migration behavior, NR6 mouse fibroblasts were seeded into CG scaffolds with pore sizes ranging from 96 to 151 μm; the migratory behavior of all cells within the imaging field of view was then tracked using 3D time-lapse confocal microscopy [82]. Tracks generated from 10 h experiments show that cells migrating in scaffolds with larger pore sizes exhibit less cell dispersion (Wind-Rose plot, Fig. 13A) and are less motile (Fig. 13B). Further quantification of these tracks shows that cell speed of the motile fraction significantly decreases with increasing scaffold pore size (Fig. 13B); cell speed is reduced almost by half over the range from 96 to 151 μm, from about 12 to 6 μm/h. Further, as cell speed was calculated (and compared) for only the motile population, which also decreased significantly with mean pore size, scaffold pore size has an even more significant influence on overall cell motility than is suggested by Fig. 13B alone.

Migration of NR6 fibroblasts in a series of DHT- and EDAC-crosslinked scaffolds of constant pore size (96 μm) but variable strut modulus (E_s: 5.3–38 MPa) was tracked and the average cell speed was plotted against scaffold strut modulus (Fig. 13B). The migration speed exhibited a subtle biphasic behavior with strut modulus, increasing (significantly) from 11 to 15 μm/h for strut moduli (E_s) between 5 and 12 MPa and then decreasing (significantly) back to 12 μm/h for strut moduli of 38 MPa. The subtle biphasic dependence of scaffold strut modulus (E_s) on cell migration speed correlates well with previous experimental and computational studies of cell motility in dense, three-dimensional materials (high degree of steric hindrances) [16,127]. However, while the influence of scaffold strut elastic modulus (E_s) on cell motility was expected, since cells were not exposed to steric hindrance in these porous, CG scaffolds, the strong dependence of cell motility on pore size was not expected. To this end, potential local variations in the micromechanical and microstructural environment of individual cells within the scaffold network were considered using experimental and cellular solids modeling tools in order to better explain the experimental results.

While the strut moduli (E_s) and scaffold relative density (ρ^*/ρ_s) are constant for the scaffolds of different pore size, considering the CG scaffold geometry using cellular solids arguments suggests that scaffolds with a larger pore size contain slightly longer and thicker struts (Fig. 3). While the moduli (E_s) of these struts is identical, the moment of inertia (I) increases with increasing pore size due to the slight increase (taken then to the fourth power) in strut thickness, translating to a larger strut flexural rigidity (E_sI) with increasing pore size. Cells have been observed to apply a constant contractile force to the CG scaffold regardless of the system stiffness [120] which suggests that cells probe their local mechanical environment by applying a constant traction force and measuring the resultant substrate deformation [128]; strut flexural rigidity is expected to be the more relevant mechanical cue to cells rather than strut modulus alone. Even though the struts have a constant Young's modulus, they may 'feel' stiffer in scaffolds with larger pore sizes because of an increased resistance to buckling. The flexural rigidity (E_sI) of the scaffold with the largest pore size (151 μm) was calculated to be greater than the scaffold with the smallest (96 μm) pore size by a factor of 6.1 (data not shown). Thus, if a mechanosensitive hypothesis, that posits the influence of scaffold pore size on motility as being due to changes in the strut flexural rigidity, were true, it would further predict that cell motility would be reduced as scaffold elastic modulus increases independent of microstructure (modifying E_s rather than I to change the overall flexural rigidity, E_sI). However, considering the results of the second experiment examining the independent influence of strut E_s on cell motility rejected this hypothesis. Strut modulus (E_s) was increased over a range (between 5.3 and 38.0 MPa; Factor: 7.2; Table 2) closely approximating the change in strut flexural rigidity with mean pore size (Factor: 6.1) [74]. However, cell speed did not decrease with increasing scaffold strut stiffness (Fig. 13B): instead cell speed exhibited the subtle biphasic dependence on strut stiffness (Fig. 13B). Therefore, the pore size-dependent changes in cell speed does not arise due to changes in apparent scaffold strut stiffness [82].

After exploring the predictions made by the cellular solids modeling regarding local scaffold mechanics, geometric insights of the cellular solids model were then used to provide potential local contact guidance cues that may explain the influence of pore size on cell motility [82]. Strut junctions, points in the scaffold microstructure where two or more struts meet, are discrete areas of significantly different extracellular morphology compared to an individual strut. With the average strut length for the different scaffolds used in the cell motility investigation of order 30–60 μm, motile cells as well as sessile cells extending processes are expected to regularly encounter strut junctions (likely multiple junctions during the 10 h imaging period used in this experiment). Two particular measurements of strut junctions were explored: strut junction spacing (D_{jxn}) and density (ρ_{jxn}, the number of strut junctions per unit cell divided by the volume of a unit cell). D_{jxn} and ρ_{jxn} of the different CG scaffold microstructures (mean pore size: 96–151 μm) can be described using the scaffold mean pore size (d) assuming a tetrakaidecahedral unit cell [76]:

$$D_{jxn} = l = \frac{d}{2.785} \tag{6}$$

$$\rho_{jxn} = \frac{6(jxns/\mathrm{UC})}{11.31 \cdot (d/2.785)^3(\mathrm{vol/UC})} = \frac{11.459}{d^3} \tag{7}$$

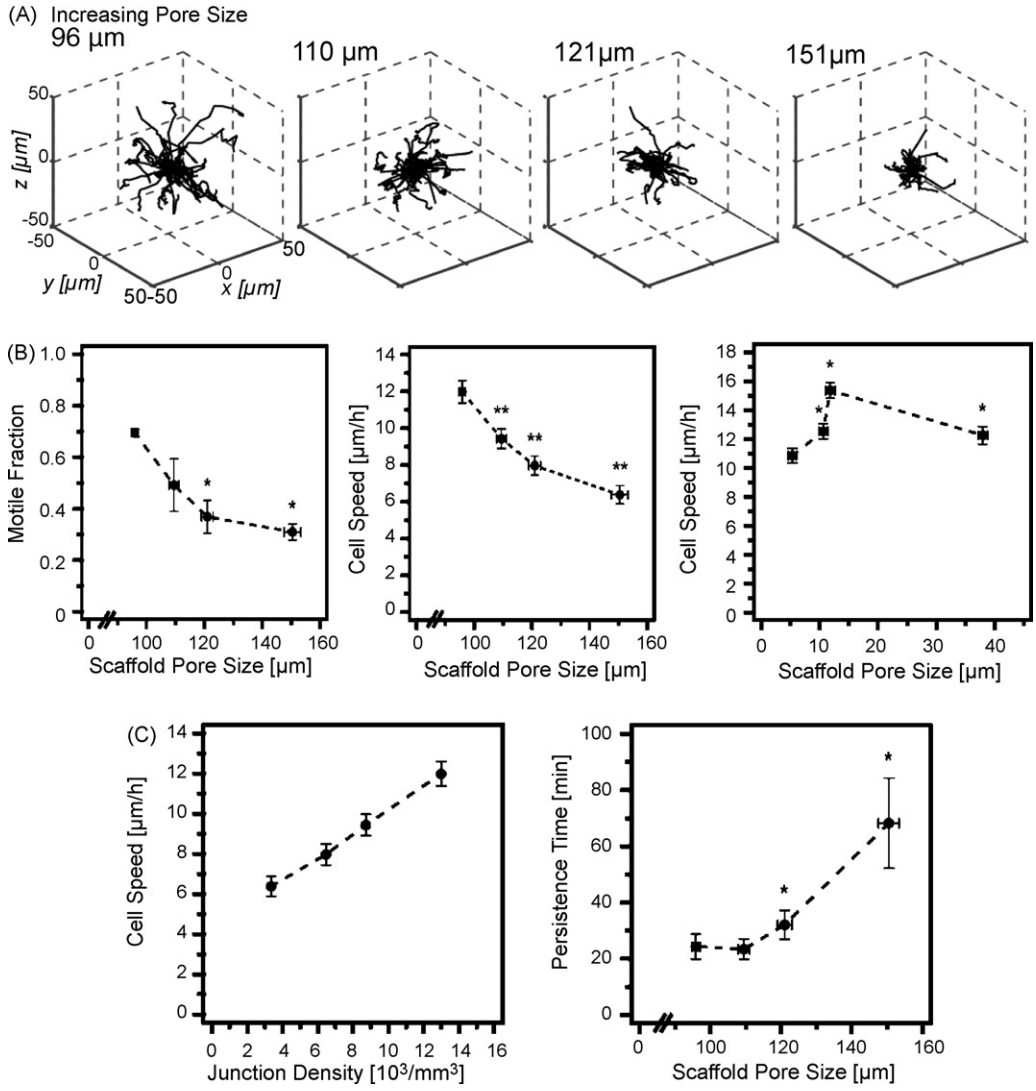

Fig. 13. (A) 3D Wind-Rose plots of randomly chosen cell tracks showing cell dispersion; cell dispersion decreases as scaffold mean pore size increases from left to right. (B) Motile fraction and mean cell speed decreases as scaffold pore size increases. Cell speed shows a biphasic relationship with scaffold strut modulus. (C) Cell speed increases proportionally with scaffold strut junction density. Cell persistence time increases with pore size (increasing distance between strut junctions). Reprinted with permission [82].

Replotting the pore size-dependent cell speed data strut junction density, an exceptionally strong correlation between cell speed and strut junction density was observed (Fig. 13C); further exploration of the potential influence of this local microstructural cue was pursued. Cells migrating in scaffolds with larger pore sizes, therefore larger D_{jxn} and lower ρ_{jxn}, were observed to exhibit greater persistence times, indicating more directional motion along a scaffold strut (Fig. 13C). In contrast, persistence times of cells migrating in scaffolds with smaller pore sizes and greater ρ_{jxn} are significantly lower, representative of erratic movement that likely occurs more often at junctions when cells can probe their local environment along multiple struts. These results provided a mechanistic explanation for our initially counter-intuitive observation that cell motility decreases as scaffold pore size increases and provide a link between junction density and cell migration behavior [82].

5. Conclusions

Porous, three-dimensional scaffolds have been used extensively for a variety of tissue engineering applications. A primary application is use as an analog of the ECM capable of inducing regeneration of damaged tissues and organs, while an important evolving application is their use as constructs to quantitatively study cell behavior and cell-scaffold interactions. Scaffold material and microstructural properties have been observed to significantly affect scaffold bioactivity and regenerative capacity [2,49]. However, the specific influence of scaffold parameters such as mechanical properties, composition, degradation characteristics, pore microstructure, and release of drugs or other soluble regulators during degradation, as well as environmental parameters such as soluble regulator (growth factors, cytokines) content, cell culture conditions, and exogenous loading is currently unknown and under investigation.

CG scaffolds are comprised of naturally derived ECM and allow investigations of highly porous and fibrous ECM systems relevant to physiology and tissue engineering applications. Fabricating CG scaffolds via freeze drying allows independent modulation of scaffold mean pore size [2], pore shape and orientation [63,129], relative density [74], mechanical properties [74], chemical composition [41,49,63,69], and available ligands. CG scaffolds have demonstrated their applicability for *in vivo* tissue regeneration in skin and nerve models and triple co-precipitated CGCaP nanocomposite scaffolds are currently being studied for bone and osteochondral applications. Additionally, uniform scaffolds with well-characterized and controllable chemical, mechanical, and microstructural properties are an ideal platform for *in vitro* studies of the effect of the extracellular matrix environment on cell behavior such as the ongoing investigation of the relationship between cell motility and cell-mediated contraction and the scaffold microenvironment. Finally, as CG scaffolds as well as many other tissue engineering scaffolds resemble low-density, open-cell foams due to their interconnected network of struts, they can be modeled as cellular solids. Implementation of such modeling techniques only increases the relevance of CG scaffolds for tissue engineering applications because it motivates further scaffold characterization and provides insight into the complex relationship between scaffold microstructural and mechanical properties. To date, cellular solids modeling have been utilized to describe CG scaffold specific surface area, permeability, mechanical properties, and have been used to aid studies of cell contraction and motility. Further applications of these techniques extend into finite element modeling of the cell-scaffold systems as well as potential modeling applications of the cell cytoskeleton.

Acknowledgements

The financial contributions of the Cambridge-MIT Institute (BAH, LJG), the Whitaker-MIT Health Science Fund Fellowship (BAH), NIH Grant DE 13053 (BAH), and the Matoula S. Salapatas Professorship at MIT (LJG) are gratefully recognized. The authors would like to acknowledge Dr. Andrew Lynn (OrthoMimetics, Inc., UK), Dr. Toby Freyman (MIT, now at Boston Scientific Inc., USA), Prof. Fergal O'Brien (Trinity College, Ireland), Professor Bill Bonfield (University of Cambridge, UK), Mary Waller (Trinity College), as well as Professor Merton Flemings, Professor Krystyn Van Vliet, Alan Schwartzman, Emilio Silva, the NanoMechanical Technology Laboratory, Kristin Myers, Matthew Wong, Professor Simona Socrate, and Professor Ioannis Yannas at MIT for the facilities and assistance that aided in completing this research.

References

[1] I.V. Yannas, Tissue and Organ Regeneration in Adults, Springer, New York, 2001.
[2] F.J. O'Brien, B.A. Harley, I.V. Yannas, L.J. Gibson, The effect of pore size on cell adhesion in collagen-GAG scaffolds, Biomaterials 26 (4) (2005) 433–441.
[3] J. Zeltinger, J.K. Sherwood, D.A. Graham, R. Mueller, L.G. Griffith, Effect of pore size and void fraction on cellular adhesion, proliferation, and matrix deposition, Tissue Eng. 7 (5) (2001) 557–572.
[4] S. Nehrer, H.A. Breinan, A. Ramappa, G. Young, S. Shortkroff, L.K. Louie, C.B. Sledge, I.V. Yannas, M. Spector, Matrix collagen type and pore size influence behavior of seeded canine chondrocytes, Biomaterials 18 (11) (1997) 769–776.
[5] M.C. Wake, C.W. Patrick Jr., A.G. Mikos, Pore morphology effects on the fibrovascular tissue growth in porous polymer substrates, Cell Transplant. 3 (4) (1994) 339–343.
[6] I.V. Yannas, E. Lee, D.P. Orgill, E.M. Skrabut, G.F. Murphy, Synthesis and characterization of a model extracellular matrix that induces partial regeneration of adult mammalian skin, Proc. Natl. Acad. Sci. U.S.A. 86 (3) (1989) 933–937.
[7] S.R. Peyton, A.J. Putnam, Extracellular matrix rigidity governs smooth muscle cell motility in a biphasic fashion, J. Cell Physiol. 204 (1) (2005) 198–209.
[8] F. Grinnell, C.H. Ho, Y.C. Lin, G. Skuta, Differences in the regulation of fibroblast contraction of floating versus stressed collagen matrices, J. Biol. Chem. 274 (2) (1999) 918–923.
[9] F. Grinnell, C.H. Ho, E. Tamariz, D.J. Lee, G. Skuta, Dendritic fibroblasts in three-dimensional collagen matrices, Mol. Biol. Cell 14 (2) (2003) 384–395.
[10] A. Engler, L. Bacakova, C. Newman, A. Hategan, M. Griffin, D. Discher, Substrate compliance versus ligand density in cell on gel responses, Biophys. J. 86 (2004) 617–628.
[11] T. Yeung, P.C. Georges, L.A. Flanagan, B. Marg, M. Ortiz, M. Funaki, N. Zahir, W. Ming, V. Weaver, P.A. Janmey, Effects of substrate stiffness on cell morphology, cytoskeletal structure, and adhesion, Cell Motil. Cytoskeleton 60 (2005) 24–34.
[12] H. Jiang, F. Grinnell, Cell-matrix entanglements and mechanical anchorage of fibroblasts in three-dimensional collagen matrices, Mol. Biol. Cell 16 (11) (2005) 5070–5076.
[13] J. Pelham, J. Robert, Y.-L. Wang, Cell locomotion and focal adhesions are regulated by substrate flexibility, Proc. Natl. Acad. Sci. U.S.A. 9 (1997) 13661–13665.
[14] T.M. Freyman, I.V. Yannas, R. Yokoo, L.J. Gibson, Fibroblast contraction of a collagen-GAG matrix, Biomaterials 22 (21) (2001) 2883–2891.
[15] D. Schulz-Torres, T.M. Freyman, I.V. Yannas, M. Spector, Tendon cell contraction of collagen-GAG matrices *in vitro*: effect of crosslinking, Biomaterials 21 (2000) 1607–1619.
[16] M.H. Zaman, L.M. Trapani, A.L. Sieminski, D. Mackellar, H. Gong, R.D. Kamm, A. Wells, D.A. Lauffenburger, P. Matsudaira, Migration of tumor cells in 3D matrices is governed by matrix stiffness along with cell-matrix adhesion and proteolysis, Proc. Natl. Acad. Sci. U.S.A. 103 (29) (2006) 10889–10894.
[17] D.W. Hutmacher, J.C. Goh, S.H. Teoh, An introduction to biodegradable materials for tissue engineering applications, Ann. Acad. Med. Singapore 30 (2) (2001) 183–191.
[18] J.F. Alvarez-Barreto, M.C. Shreve, P.L. Deangelis, V.I. Sikavitsas, Preparation of a functionally flexible, three-dimensional, biomimetic poly(L-lactic acid) scaffold with improved cell adhesion, Tissue Eng. 13 (6) (2007) 1205–1217.
[19] A.R. Webb, J. Yang, G.A. Ameer, Biodegradable polyester elastomers in tissue engineering, Expert Opin. Biol. Ther. 4 (6) (2004) 801–812.
[20] S. Wang, W. Cui, J. Bei, Bulk and surface modifications of polylactide, Anal. Bioanal. Chem. 381 (3) (2005) 547–556.
[21] J.K. Tessmar, A.M. Gopferich, Customized PEG-derived copolymers for tissue-engineering applications, Macromol. Biosci. 7 (1) (2007) 23–39.
[22] E. Sachlos, J.T. Czernuszka, Making tissue engineering scaffolds work. Review: the application of solid freeform fabrication technology to the production of tissue engineering scaffolds, Eur. Cell Mater. 5 (2003) 29–39, discussion 39–40.
[23] D.R. Carter, D.M. Spengler, Mechanical Properties and Composition of Cortical Bone, Clin. Orthop. Relat. Res. 135 (1978) 192–217.
[24] R.Z. LeGeros, Properties of Osteoconductive Biomaterials: Calcium Phosphates, Clin. Orthop. Relat. Res. 395 (2002) 81–98.

[25] B. Doll, C. Sfeir, S. Winn, J. Huard, J. Hollinger, Critical aspects of tissue-engineered therapy for bone regeneration, Crit. Rev. Eukaryot. Gene Expr. 11 (2001) 173–198.
[26] C.P. Klein, A.A. Driessen, K. de Groot, A. van den Hooff, Biodegradation behavior of various calcium phosphate materials in bone tissue, J. Biomed. Mater. Res. 17 (5) (1983) 769–784.
[27] J.L. Ong, D.C.N. Chan, Hydroxyapatite and their use as coatings in dental implants: a review, Crit. Rev. Biomed. Eng. 28 (5/6) (2000) 667A–707A.
[28] S. Overgaard, Calcium phosphate coatings for fixation of bone implants—evaluated mechanically and histologically by stereological methods, Acta Orthop. Scand. 71 (6 (Suppl. 297)) (2000) 1–74.
[29] S.D. Boden, J.H. Schimandle, Biologic enhancement of spinal fusion, Spine 20 (24) (1995) S113–S123.
[30] W. Bonfield, M.D. Grynpas, A.E. Tully, J. Bowman, J. Abram, Hydroxyapatite reinforced polyethylene—a mechanically compatible implant material for bone replacement, Biomaterials 2 (3) (1981) 185–186.
[31] G. Geyer, Materials for middle ear reconstruction, HNO 47 (2) (1999) 77–91.
[32] H. Benebassath, B.Y. Klein, E. Lermer, R. Azoury, E. Rahamim, Z. Shlomai, S. Sarig, An *in-vitro* biocompatibility study of a new hydroxyapatite ceramic HA-SAL1—comparison to bioactive bone substitute ceramics, Cells Mater. 4 (1994) 37–50.
[33] K. Hasegawa, S. Yamamura, Y. Dohmae, Enhancing screw stability in osteosynthesis with hydroxyapatite granules, Arch. Orthop. Trauma Surg. 117 (1998) 175–176.
[34] M. Bohner, Calcium orthophosphates in medicine: from ceramics to calcium phosphate cements, Injury 31 (Suppl. 4) (2000) 37–47.
[35] A. Moreira-Gonzalez, I.T. Jackson, T. Miyawaki, V. DiNick, R. Yavuzer, Augmentation of the craniomaxillofacial region using porous hydroxyapatite granules, Plast. Reconstr. Surg. 111 (2003) 1808–1817.
[36] A.R. Boccaccini, J.J. Blaker, Bioactive composite materials for tissue engineering scaffolds, Expert Rev. Med. Devices 2 (3) (2005) 303–317.
[37] V. Maquet, A.R. Boccaccini, L. Pravata, I. Notingher, R. Jerome, Preparation, characterization, and *in vitro* degradation of bioresorbable and bioactive composites based on Bioglass-filled polylactide foams, J. Biomed. Mater. Res. 66A (2) (2003) 335–346.
[38] C.V. Brovarone, E. Verne, P. Appendino, Macroporous bioactive glass-ceramic scaffolds for tissue engineering, J. Mater. Sci. Mater. Med. 17 (11) (2006) 1069–1078.
[39] C. Vitale-Brovarone, E. Verne, L. Robiglio, P. Appendino, F. Bassi, G. Martinasso, G. Muzio, R. Canuto, Development of glass-ceramic scaffolds for bone tissue engineering: characterisation, proliferation of human osteoblasts and nodule formation, Acta Biomater. 3 (2) (2007) 199–208.
[40] H.W. Kim, J.H. Song, H.E. Kim, Bioactive glass nanofiber-collagen nanocomposite as a novel bone regeneration matrix, J. Biomed. Mater. Res. A 79 (3) (2006) 698–705.
[41] A.K. Lynn, S.M. Best, R.E. Cameron, B.A. Harley, I.V. Yannas, L.J. Gibson, W. Bonfield, Design of a multiphase osteochondral scaffold II: control of chemical composition, J. Biomed. Mater. Res. A, 2007, in review.
[42] A.K. Lynn, B.A. Harley, I.V. Yannas, N. Rushton, M. Spector, L.J. Gibson, W. Bonfield, Design of an osteochondral scaffold I: basic design principles, J. Biomed. Mater. Res. B, 2007, in review.
[43] H.M. Kim, Bioactive ceramics: challenges and perspectives, J. Ceram. Soc. Jpn. 109 (4) (2001) S49–S57.
[44] A.K. Lynn, I.V. Yannas, W. Bonfield, Antigenicity and immunogenicity of collagen, J. Biomed. Mater. Res. B Appl. Biomater. 71 (2) (2005) 343–354.
[45] I.V. Yannas, J.F. Burke, C. Huang, P.L. Gordon, Suppression of *in vivo* degradability and of immunogenicity of collagen by reaction with glycosaminoglycans, Polym. Prep. Am. Chem. Soc. 16 (2) (1975) 209–214.
[46] T.M. Freyman, I.V. Yannas, L.J. Gibson, Cellular materials as porous scaffolds for tissue engineering, Prog. Mater. Sci. 46 (2001) 273–282.
[47] K.K. Sethi, I.V. Yannas, V. Mudera, M. Eastwood, C. McFarland, R.A. Brown, Evidence for sequential utilization of fibronectin, vitronectin, and collagen during fibroblast-mediated collagen contraction, Wound Repair Regen. 10 (6) (2002) 397–408.
[48] I.V. Yannas, Biologically-active analogs of the extracellular-matrix—artificial skin and nerves, Angew. Chem. Int. Ed. English 29 (1) (1990) 20–35.
[49] B.A. Harley, M.H. Spilker, J.W. Wu, K. Asano, H.P. Hsu, M. Spector, I.V. Yannas, Optimal degradation rate for collagen chambers used for regeneration of peripheral nerves over long gaps, Cells Tissues Organs 176 (1–3) (2004) 153–165.
[50] C.C. Tsai, S.D. Lin, C.S. Lai, T.M. Lin, The use of composite acellular allodermis-ultrathin autograft on joint area in major burn patients—one year follow-up, Kaohsiung, J. Med. Sci. 15 (11) (1999) 651–658.
[51] S.F. Badylak, The extracellular matrix as a biologic scaffold material, Biomaterials 28 (25) (2007) 3587–3593.
[52] Y. Sasano, S. Kamakura, M. Nakamura, O. Suzuki, I. Mizoguchi, H. Akita, M. Kagayama, Subperiosteal implantation of octacalcium phosphate (OCP) stimulates both chondrogenesis and osteogenesis in the Tibia, but only osteogenesis in the parietal bone of a rat, Anat. Rec. 242 (1) (1995) 40–46.
[53] J. Hemmerle, M. Leize, J.C. Voegel, Long-term behavior of a hydroxyapatite collagen-glycosaminoglycan biomaterial used for oral-surgery—a case-report, J. Mater. Sci. Mater. Med. 6 (6) (1995) 360–366.
[54] G.F. Muschler, S. Negami, A. Hyodo, D. Gaisser, K. Easley, H. Kambic, Evaluation of collagen ceramic composite graft materials in a spinal fusion model, Clin. Orthop. Relat. Res. 328 (1996) 250–260.
[55] D.R. Mehlisch, A.S. Leider, W.E. Roberts, Histologic evaluation of the bone-graft interface after mandibular augmentation with hydroxylapatite purified fibrillar collagen composite implants, Oral Surg. Oral Med. Oral Pathol. Oral Radiol. Endod. 70 (6) (1990) 685–692.
[56] K.S. Ten Huisen, R.I. Martin, M. Klimkiewicz, P.W. Brown, Formation, Properties of a synthetic bone composite: hydroxyapatite-collagen, J. Biomed. Mater. Res. 29 (7) (1995) 803–810.
[57] M. Kikuchi, S. Itoh, S. Ichinose, K. Shinomiya, J. Tanaka, Self-organization mechanism in a bone-like hydroxyapatite/collagen nanocomposite synthesized *in vitro* and its biological reaction *in vivo*, Biomaterials 22 (13) (2001) 1705–1711.
[58] S.H. Rhee, Y. Suetsugu, J. Tanaka, Biomimetic configurational arrays of hydroxyapatite nanocrystals on bio-organics, Biomaterials 22 (21) (2001) 2843–2847.
[59] A.K. Lynn, R.E. Cameron, S.M. Best, R.A. Brooks, N. Rushton, W. Bonfield, Phase mapping: a novel design approach for the production of calcium phosphate-collagen biocomposites, Key Eng. Mater. 254–256 (2004) 593–596.
[60] A.K. Lynn, T. Nakamura, N. Patel, A.E. Porter, A.C. Renouf, P.R. Laity, S.M. Best, R.E. Cameron, Y. Shimizu, W. Bonfield, Composition-controlled nanocomposites of apatite and collagen incorporating silicon as an osseopromotive agent, J. Biomed. Mater. Res. Part A 74 (3) (2005) 447–453.
[61] A.I. Martin, A.J. Salinas, M. Vallet-Regi, Bioactive and degradable organic-inorganic hybrids, J. Eur. Ceram. Soc. 25 (16) (2005) 3533–3538.
[62] K. Kataoka, Y. Nagao, T. Nukui, I. Akiyama, K. Tsuru, S. Hayakawa, A. Osaka, N.H. Huh, An organic-inorganic hybrid scaffold for the culture of HepG2 cells in a bioreactor, Biomaterials 26 (15) (2005) 2509–2516.
[63] F.J. O'Brien, B.A. Harley, I.V. Yannas, L. Gibson, Influence of freezing rate on pore structure in freeze-dried collagen-GAG scaffolds, Biomaterials 25 (6) (2004) 1077–1086.
[64] B.A. Harley, M.C. Flemings, Coarsening-mediated solidification is responsible for defining the pore microstructure of collagen-glycosaminoglycan scaffolds: experimental and thermal modeling results, Acta Mater., in revision.
[65] L.J. Chamberlain, I.V. Yannas, Preparation of collagen-glycosaminoglycan copolymers for tissue regeneration, in: J.R. Morgan, M.L. Yarmush (Eds.), Methods of Molecular Medicine, Humana Press, Tolowa, NJ, 1998.
[66] L.J. Chamberlain, I.V. Yannas, H.-P. Hsu, G. Strichartz, M. Spector, Collagen-GAG substrate enhances the quality of nerve regeneration through collagen tubes up to level of autograft, Exp. Neurol. 154 (1998) 315–329.
[67] L.J. Chamberlain, I.V. Yannas, A. Arrizabalaga, H.P. Hsu, T.V. Norregaard, M. Spector, Early peripheral nerve healing in collagen and silicone

tube implants: myofibroblasts and the cellular response, Biomaterials 19 (15) (1998) 1393–1403.
[68] B.A. Harley, A.Z. Hastings, I.V. Yannas, A. Sannino, Fabricating tubular scaffolds with a radial pore size gradient by a spinning technique, Biomaterials 27 (6) (2006) 866–874.
[69] B.A. Harley, A.K. Lynn, Z. Wissner-Gross, W. Bonfield, I.V. Yannas, L.J. Gibson, Design of a multiphase osteochondral scaffold III: fabrication of a mineralized collagen-GAG scaffold, J. Biomed. Mater. Res. A, 2007, in review.
[70] A.K. Lynn, W. Bonfield, A novel method for the simultaneous, titrant-free control of pH and calcium phosphate mass yield, Acc. Chem. Rev. 38 (3) (2005) 202–207.
[71] B.A. Harley, A.K. Lynn, Z. Wissner-Gross, W. Bonfield, I.V. Yannas, L.J. Gibson, Design and fabrication of a multiphase osteochondral scaffold, in: Proc. First Int. Conf. on Mech. of Biomaterials & Tissues; 2005, 2005.
[72] B.A. Harley, A.K. Lynn, Z. Wissner-Gross, W. Bonfield, I.V. Yannas, L.J. Gibson, Design of a multiphase osteochondral scaffold IV: fabrication of layered scaffolds with soft interfaces, J. Biomed. Mater. Res. A, 2007, in review.
[73] I.V. Yannas, A.V. Tobolsky, Cross linking of gelatine by dehydration, Nature 215 (100) (1967) 509–510.
[74] B.A. Harley, J.H. Leung, E.C.C.M. Silva, L.J. Gibson, Mechanical characterization of collagen-GAG scaffolds, Acta Biomater. 3 (4) (2007) 463–474.
[75] B.A. Harley, T.M. Freyman, M.Q. Wong, L.J. Gibson, A new technique for calculating individual dermal fibroblast contractile forces generated within collagen-GAG scaffolds, Biophys. J. 93 (8) (2007) 2911–2922.
[76] L.J. Gibson, M.F. Ashby, Cellular Solids: Structure and Properties, second ed., Cambridge University Press, Cambridge, UK, 1997.
[77] R.E. Williams, Space-filling polyhedron: its relation to aggregates of soap bubbles, plant cells and metal crystallites, Science 161 (1968) 276–277.
[78] W. Thompson, On the division of space with minimum partition energy, Phil. Mag. 24 (1887) 503.
[79] A.M. Kraynik, D.A. Reinelt, F. van Swol, Structure of random monodisperse foam, Phys. Rev. 67 (2003) 031403.
[80] J.R. Levick, Flow through interstitium and other fibrous matrices, Q. J. Exp. Physiol. 72 (4) (1987) 409–437.
[81] F.J. O'Brien, B.A. Harley, M.A. Waller, I.V. Yannas, L.J. Gibson, P.J. Prendergast, The effect of pore size on permeability and cell attachment in collagen scaffolds for tissue engineering, Technol. Health Care 15 (1) (2007) 3–17.
[82] B.A. Harley, H.-D. Kim, M.H. Zaman, I.V. Yannas, D.A. Lauffenburger, L.J. Gibson, Micro-architecture of three-dimensional scaffolds infleunces cell migration behavior via junction interactions, Biophys. J., 2007, in review.
[83] E. Farrell, F.J. O'Brien, E. Byrne, P. Doyle, J. Fischer, I.V. Yannas, B.A. Harley, B. O'Connell, P.J. Prendergast, V.A. Campbell, A collagen-glycosaminoglycan scaffold supports adult rat mesenchymal stem cell differentiation along the osteogenic and chrondrogenic routes, Tissue Eng. 12 (3) (2006) 459–468.
[84] C.C. Compton, C.E. Butler, I.V. Yannas, G. Warland, D.P. Orgill, Organized skin structure is regenerated *in vivo* from collagen-GAG matrices seeded with autologous keratinocytes, J. Invest. Dermatol. 110 (6) (1998) 908–916.
[85] B.A. Harley, I.V. Yannas, Induced peripheral nerve regeneration using scaffolds, Minerva Biotechnol. 18 (2) (2006) 97–120.
[86] A.S. Chang, I.V. Yannas, S. Perutz, H. Loree, R.R. Sethi, C. Krarup, T. Norregaard, N.T. Zervas, J. Silver, Electrophysiological study of recovery of peripheral nerves regenerated by a collagen-glycosaminoglycan copolymer matrix, in: R.L. Dunn (Ed.), Progress in Biomedical Polymers, Plenum Press, New York, 1990, pp. 107–119.
[87] L.J. Chamberlain, I.V. Yannas, H.P. Hsu, G.R. Strichartz, M. Spector, Near-terminus axonal structure and function following rat sciatic nerve regeneration through a collagen-GAG matrix in a ten-millimeter gap, J. Neurosci. Res. 60 (5) (2000) 666–677.
[88] R.E. Samuel, C.R. Lee, S.C. Ghivizzani, C.H. Evans, I.V. Yannas, B.R. Olsen, M. Spector, Delivery of plasmid DNA to articular chondrocytes via novel collagen-glycosaminoglycan matrices, Hum. Gene Ther. 13 (7) (2002) 791–802.
[89] R.M. Capito, M. Spector, Scaffold-based articular cartilage repair, IEEE Eng. Med. Biol. Mag. 22 (5) (2003) 42–50.
[90] C.R. Lee, A.J. Grodzinsky, H.-P. Hsu, M. Spector, Effects of a cultured autologous chondrocyte-seeded type II collagen scaffold on the healing of a chondral defect in a canine model, J. Orthop. Res. 21 (2003) 272–281.
[91] B. Kinner, R.M. Capito, M. Spector, Regeneration of articular cartilage, Adv. Biochem. Eng. Biotechnol. 94 (2005) 91–123.
[92] S.M. Vickers, L.S. Squitieri, M. Spector, The effects of cross-linking type II collagen-GAG scaffolds on chondrogenesis *in vitro*: dynamic pore reduction promotes cartilage formation, Tissue Eng. 12 (5.) (2006).
[93] R.M. Capito, M. Spector, Collagen scaffolds for nonviral IGF-1 gene delivery in articular cartilage tissue engineering, Gene Ther. 14 (9) (2007) 721–732.
[94] A.F. Steinert, G.D. Palmer, R. Capito, J.G. Hofstaetter, C. Pilapil, S.C. Ghivizzani, M. Spector, C.H. Evans, Genetically enhanced engineering of meniscus tissue using ex vivo delivery of transforming growth factor-beta1 complementary deoxyribonucleic acid, Tissue Eng. 13 (9) (2007) 2227–2237.
[95] L. Saad, M. Spector, Effects of collagen type on the behavior of adult canine annulus fibrosus cells in collagen-glycosaminoglycan scaffolds, J. Biomed. Mater. Res. A 71 (2) (2004) 233–241.
[96] A.K. Lynn, B.A. Harley, Z. Wissner-Gross, I.V. Yannas, L.J. Gibson, W. Bonfield, Design and fabrication of a mineralized, triple-co-precipitate collagen-glycosaminoglycan scaffold, in: Proc. First Intl. Conf. on Mech. of Biomaterials & Tissues; 2005, 2005.
[97] J. Jaworski, C.M. Klapperich, Fibroblast remodeling activity at two- and three-dimensional collagen-glycosaminoglycan interfaces, Biomaterials 27 (23) (2006) 4212–4220.
[98] J. Lee, M. Leonard, T. Oliver, A. Ishihara, K. Jacobson, Traction forces generated by locomoting keratocytes, J. Cell. Biol. 127 (1994) 1957–1964.
[99] P. Roy, W.M. Petroll, C.J. Chuong, H.D. Cavanagh, J.V. Jester, Effect of cell migration on the maintenance of tension on a collagen matrix, Ann. Biomed. Eng. 27 (1999) 721–730.
[100] Harris, Silicone rubber substrata: a new wrinkle in the study of cell locomotion, Science 208 (1980) 177–179.
[101] T. Oliver, M. Dembo, K. Jacobson, Traction forces in locomoting cells, Cell Motil. Cytoskeleton 31 (1995) 225–240.
[102] M. Dembo, Y.-L. Wang, Stresses at the cell-to-substrate interface during locomotion of fibroblasts, Biophys. J. 76 (1999) 2307–2316.
[103] J.L. Tan, J. Tien, D.M. Pirone, D.S. Gray, K. Bhadriraju, C.S. Chen, Cells lying on a bed of microneedles: an approach to isolate mechanical force, Proc. Natl. Acad. Sci. U.S.A. 100 (4) (2003) 1484–1489.
[104] C.A. Lemmon, N.J. Sniadecki, S.A. Ruiz, J.L. Tan, L.H. Romer, C.S. Chen, Shear force at the cell-matrix interface: enhanced analysis for microfabricated post array detectors, Mech. Chem. Biosyst. 2 (1) (2005) 1–16.
[105] P. Roy, W.M. Petroll, H.D. Cavanagh, C.J. Chuong, J.V. Jster, An *in vitro* force measurement assay to study the early mechanical interaction between corneal fibroblasts and collagen matrix, Exp. Cell Res. 232 (1997) 106–117.
[106] S. Munevar, Y. Wang, M. Dembo, Traction force microscopy of migrating normal and H-ras transformed 3T3 fibroblasts, Biophys. J. 80 (4) (2001) 1744–1757.
[107] S. Munevar, Y.-L. Wang, M. Dembo, Distinct roles of frontal and rear cell-substrate adhesions in fibrolast migration, Mol. Biol. Cell 12 (2001) 3947–3954.
[108] C.-M. Lo, H.-B. Wang, M. Dembo, Y.-L. Wang, Cell movement is guided by the rigidity of the substrate, Biophys. J. 79 (2000) 144–152.
[109] C.S. Chen, D.E. Ingber, Tensegrity and mechanoregulation: from skeleton to cytoskeleton, Osteoarthritis Cartilage 7 (1999) 81–94.
[110] N. Wang, J.P. Butler, D. Ingber, Mechanotransduction across the cell surface and through the cytoskeleton, Science 260 (1993) 1124–1127.
[111] H.-B. Wang, M. Dembo, Y.-L. Wang, Substrate flexibility regulates growth and apoptosis of normal but not transformed cells, Am. J. Physiol. Cell Physiol. 279 (2000) C1345–C1350.

[112] K.A. Beningo, M. Dembo, I. Kaverina, J.V. Small, Y.-L. Wang, Nascent focal adhesions are responsible for the generation of strong propulsive forces in migrating fibroblasts, J. Cell Biol. 153 (4) (2001) 881–887.
[113] H.-B. Wang, M. Dembo, S.K. Hanks, Y.-L. Wang, Focal adhesion kinase is involved in mechanosensing during fibroblast migration, Proc. Natl. Acad. Sci. U.S.A. 98 (20) (2001) 11295–11300.
[114] K.A. Beningo, Y.-L. Wang, Flexible substrata for the detection of cellular traction forces, Trends Cell Biol. 12 (2) (2002) 79–84.
[115] A.J. Engler, S. Sen, H.L. Sweeney, D.E. Discher, Matrix elasticity directs stem cell lineage specification, Cell 126 (4) (2006) 677–689.
[116] J.P. Marquez, G.M. Genin, G.I. Zahalak, E.L. Elson, The relationship between cell and tissue strain in three-dimensional bio-artificial tissues, Biophys. J. 88 (2) (2005) 778–789.
[117] F. Guilak, G.R. Erickson, H.P. Ting-Beall, The effects of osmotic stress on the viscoelastic and physical properties of articular chondrocytes, Biophys. J. 82 (2) (2002) 720–727.
[118] G.I. Zahalak, J.E. Wagenseil, T. Wakatsuki, E.L. Elson, A cell-based constitutive relation for bio-artificial tissues, Biophys. J. 79 (5) (2000) 2369–2381.
[119] T.M. Freyman, I.V. Yannas, Y.-S. Pek, R. Yokoo, L.J. Gibson, Micromechanics of fibroblast contraction of a collagen-GAG matrix, Exp. Cell. Res. 269 (2001) 140–153.
[120] T.M. Freyman, I.V. Yannas, R. Yokoo, L.J. Gibson, Fibroblast contractile force is independent of the stiffness which resists the contraction, Exp. Cell Res. 272 (2) (2002) 153–162.
[121] T.C. Triantafillou, J. Zhang, T.L. Shercliff, L.J. Gibson, M.F. Ashby, Failure surfaces for cellular materials under multiaxial loads. 2. Comparison of models with experiment, Int. J. Mech. Sci. 31 (9) (1989) 665–678.
[122] D.A. Lauffenburger, A.F. Horwitz, Cell migration: a physically integrated molecular process, Cell 84 (3) (1996) 359–369.
[123] P. Friedl, K.S. Zanker, E.B. Brocker, Cell migration strategies in 3-D extracellular matrix: differences in morphology, cell matrix interactions, and integrin function, Microsc. Res. Tech. 43 (5) (1998) 369–378.
[124] J. Condeelis, J.E. Segall, Intravital imaging of cell movement in tumours, Nat. Rev. Cancer 3 (12) (2003) 921–930.
[125] T. Lapidot, A. Dar, O. Kollet, How do stem cells find their way home? Blood 106 (6) (2005) 1901–1910.
[126] A. Wilson, A. Trumpp, Bone-marrow haematopoietic-stem-cell niches, Nat. Rev. Immunol. 6 (2) (2006) 93–106.
[127] M.H. Zaman, R.D. Kamm, P. Matsudaira, D.A. Lauffenburger, Computational model for cell migration in three-dimensional matrices, Biophys. J. 89 (2) (2005) 1389–1397.
[128] V. Vogel, M. Sheetz, Local force and geometry sensing regulate cell functions, Nat. Rev. Mol. Cell. Biol. 7 (4) (2006) 265–275.
[129] H.M. Loree, I.V. Yannas, B. Mikic, A.S. Chang, S.M. Perutz, T.V. Norregaard, C. Krarup, A freeze-drying process for fabrication of polymeric bridges for peripheral nerve regeneration, in: Proc. 15th Annual Northeast Bioeng. Conf.; 1989, 1989, pp. 53–54.
[130] Y.S. Pek, M. Spector, I.V. Yannas, L.J. Gibson, Degradation of a collagen-chondroitin-6-sulfate matrix by collagenase and by chondroitinase, Biomaterials 25 (3) (2004) 473–482.